The curdlan and/or anti-VISTA monoclonal antibody enhances innate and adaptive immune responses in the mouse model of melanoma

by

Siavash Mashhouri

A thesis submitted in partial fulfillment of the requirements for the degree of

Master of Science

Medical Sciences - Oral Biology
University of Alberta

Abstract

During the past decade, the field of immuno-oncology has been revolutionized by the emergence of immune checkpoint inhibitors (ICIs). However, acquired resistance to ICIs and relapse after immunotherapy are associated with defects in antigen presentation and the upregulation of exhaustion ligands in tumours. Therefore, identifying new approaches to overcome these barriers is crucial to improve the quality of life and increase the survival rate in cancer patients. Dendritic cell-associated C-type lectin-1 (Dectin-1) is a C-type lectin receptor best known for its ability to recognize β-glucan-rich structures in fungal cell walls. Dectin-1 is expressed in myeloid cells and tumour cells, however, its role in cancer has been the subject of debate and controversy. Therefore, I decided to investigate the role of Dectin-1 in B16-F10 melanoma and CT26 colorectal tumour models. I found that myeloid cells were the most dominant cells in terms of Dectin-1 expression. In particular, I found that Dectin-1+ myeloid cells exhibited an activated phenotype characterized by elevated levels of CD80, CD86, and MHC Class II levels in the tumour microenvironment (TME). For the very first time, based on my knowledge, observed a strong co-expression/co-localization of Dectin-1 with V-domain Ig suppressor of T cell activation (VISTA), Programmed death-ligand 1 (PD-L1), Programmed death-ligand 1 (PD-L2), and T-cell immunoglobulin and mucin-domain containing-3 (TIM-3) in myeloid cells from the TME versus spleen in tumor-bearing mice. Our results indicated that Dectin-1 is commonly expressed by active tumor-associated myeloid cells. However, I found significantly greater levels of Dectin-1 at the gene and protein levels in myeloid cells from the B16-F10 model. Therefore, I decided to further investigate the role of Dectin-1 in the B16-F10 model by deleting this molecule (using Dectin-1 knockout) or stimulating Dectin-1 by treating mice with curdlan (a β-glucan ligand. Although Dectin-1 deletion had no effects on tumor progression, curdlan treatment significantly enhanced the innate and adaptive immune responses resulting in reduced tumor progression. Therefore, Dectin-1

stimulation could be considered a potential target concurrent with ICIs since it engages innate and adaptive immune responses. These results provide more justification for designing novel immunotherapy strategies by reprogramming the TME to target both arms of the immune system.

Preface

Ethics Approval

This thesis is an original work by Siavash Mashhouri. The research project, of which this thesis is a part, was conducted under the recommendations in the Guide for the Care and Use of Laboratory Animals of the Canadian Council for Animal Care. The protocol was approved by the Animal Ethics Boards of the University of Alberta (Protocol # AUP00002737).

Acknowledgment

I would like to thank my esteemed supervisor -Prof. Shokrollah Elahi- for his support during the course of my M.Sc. degree. My gratitude extends to my committee members, Dr. John Walker and Dr. Ismail Ismail for their immense knowledge and plentiful experience that have encouraged me throughout my academic research program. I would also like to thank my lab mates for their technical support and advice throughout my research. Finally, I would like to express my gratitude to my parents, my one and only sister and my beloved partner. Without their tremendous understanding and encouragement in the past three years, this would have been impossible for me to complete smoothly.

I also would like to acknowledge the Canadian Institutes of Health Research (CIHR) for supporting the Elahi lab and subsequently my research program.

Table of Contents

List of Tables

List of Figures

List of Publications

2021

Mashhouri S, Koleva P, Huynh M, Okoye I, Shahbaz S, Elahi S. Sex Matters: Physiological Abundance of Immuno-Regulatory CD71+ Erythroid Cells Impair Immunity in Females. Front Immunol. 2021 Jul 21;12:705197. doi: 10.3389/fimmu.2021.705197. PMID: 34367164; PMCID: PMC8334724.

Lee K, Elahi S, **Mashhouri S**, Ye C. Gout Presenting as a Chronic Inflammatory Arthritis from Immune Checkpoint Inhibitors: Case Series. Rheumatology (Oxford). 2021 Jul 28:keab608. doi: 10.1093/rheumatology/keab608. Epub ahead of print. PMID: 34320630.

Bozorgmehr N, **Mashhouri S**, Perez Rosero E, Xu L, Shahbaz S, Sligl W, Osman M, Kutsogiannis DJ, MacIntyre E, O'Neil CR, Elahi S. Galectin-9, a Player in Cytokine Release Syndrome and a Surrogate Diagnostic Biomarker in SARS-CoV-2 Infection. mBio. 2021 May 4;12(3):e00384-21. doi: 10.1128/mBio.00384-21. PMID: 33947753; PMCID: PMC8262904.

Shahbaz S, Xu L, Sligl W, Osman M, Bozorgmehr N, **Mashhouri S**, Redmond D, Perez Rosero E, Walker J, Elahi S. The Quality of SARS-CoV-2-Specific T Cell Functions Differs in Patients with Mild/Moderate versus Severe Disease, and T Cells Expressing Coinhibitory Receptors Are Highly Activated. J Immunol. 2021 Aug 15;207(4):1099-1111. doi: 10.4049/jimmunol.2100446. Epub 2021 Jul 26. PMID: 34312258.

2019

Elahi S, **Mashhouri S**. Immunological consequences of extramedullary erythropoiesis: immunoregulatory functions of CD71+ erythroid cells. Haematologica. 2020 Jun;105(6):1478-1483. doi: 10.3324/haematol.2019.243063. Epub 2020 Apr 30. PMID: 32354873; PMCID: PMC7271582.

Introduction

Immunotherapy

Resembling any established therapeutical approach, immunotherapy has gone through many ups and downs throughout the history. In the late 19th century, Wilhelm Busch and Friedrich Fehleisen for the first time noticed spontaneous regression of tumors following the development of erysipelas (a common type of superficial skin infections caused by group A streptococcal bacteria) in cancer patients. Later, William B. Coley, known as the father of immunotherapy, suspected that erysipelas germs might be responsible for tumor shrinkage in such patients. To test his hypothesis, he intentionally infected a couple of his cancer patients with mixture of different Streptococcus bacteria. Following couples of trials and errors, he found that *Streptococcus pyogenes* and *Serratia marcescens* are main species responsible for tumor shrinkage following in cancer patients. Therefore, he suggested that heat-killed *Streptococcus pyogenes* and *Serratia marcescens*, known as Coley's toxin could be used as a strong remedy in cancer patients. Although shrinkage of the tumor mass following deliberate injection of bacterial products (erythrogenic toxins from *Streptococcus pyogenes* and lipopolysaccharide from *Serratia marcescens*) reduced tumor size in some patients (mainly sarcoma patients), a higher risk of developing sepsis in some patients with debilitated immune system and ineffectiveness of the treatment against other types of cancer ultimately resulted in a reluctance to use this treatment(1). Although Coley's toxin gradually disappeared from the cancer therapy toolbox, understanding the mechanism of action of Coley's toxin initiated a big revolution in the field of immunotherapy. Significant advances in immunology and formation of major conceptual paradigms in immuno-oncology incited many scientists to employ immune system as a potent tool for treatment of cancer. For instance, in the 1950s, systemic administration of biological response modifiers like recombinant interleukin-2 (IL-2) or interferons-alpha (IFN-α) received huge attention in cancer immunotherapy (2)(3)(4)(5). As its name indicates, these modifiers target specific group of immune cells and proteins to mimic natural immune responses against tumor cells. Although systemic infusion of such molecules improved immune responses in some types of cancer and resulted in smaller tumors, today it is well known that systemic therapies with biological response modifiers can cause significant cytotoxicity in patients and also might increase the risk of developing autoimmune diseases (6)(7). Therefore, by the beginning of 21st century, the field of immunotherapy has been mainly focused on the cellular

components of the immune system. For example, therapeutic cancer vaccines, T cell transfer therapy and immune checkpoint inhibitors are the major areas of study in modern immunotherapy. Unlike cancer prophylactic vaccines used to prevent cancer development in healthy individuals, therapeutic cancer vaccines are used to boost adaptive immune responses against specific tumor antigens(8). The idea behind therapeutic cancer vaccines is presenting the tumor antigens to immune cells in the hope of that T cells get activated and react to tumor cells. Therefore, several approaches have been developed to deliver tumor antigens like tumor-specific protein vaccines, tumor-specific mRNA vaccines, dendritic cell vaccines and oncolytic virus therapy(8)(9)(10). Like conventional vaccines, former strategies deliver tumor antigens or cognate mRNA to antigen-presentation cells (APCs). The APCs then uptake proteins/mRNA and subsequently present them to cytotoxic T cell lymphocytes (CTLs) (10)(11). In the case of dendritic cell vaccines, patients' peripheral dendritic cells are extracted in a leukapheresis procedure and then get activated in the presence of tumor antigens and granulocyte-macrophage colony stimulating factor (GM-CSF). The activated cells later will be returned to patients through infusion (12)(13). The oncolytic virus therapy is another format of the therapeutic cancer vaccine that selectively kill infected tumor cells *in situ* that consequently results in release of a broad array of tumor antigens and danger signals in TME. Exposure of tumor-associated immune cells to tumor antigens and cellular components ultimately leads to indirect killing phase of therapy following activation of innate and adaptive cells in TME(14). Although cancer vaccine therapy is theoretically a feasible approach for stimulating immune system in cancer patients but, studies have shown that they are not as effective, possibly because of barriers to delivery of vaccine into the tumor tissues and immunosuppressive mechanisms evolve over the cancer establishment (15)(16). Furthermore, due to nature of the disease and side effects of cancer treatments, immune system might not be able to mount natural responses to the vaccines(17). Since tumor-infiltrating lymphocytes (TILs) are recognized as the main effector cells in antitumor immune responses, studies in immunotherapy have been gradually shifted to T cell therapy and immune checkpoint inhibitors (ICIs) from 2020. The autologous adoptive transfer of tumor-infiltrating lymphocytes (TILs), engineered T cells and tumor-specific chimeric antigen receptor T cells (CAR-T) are examples of successful cell therapies in the field of immunotherapy over the past decade (18)(19)(20). Unlike therapeutic cancer vaccines that target APCs, T cell therapy strategies targets CTLs. In autologous adoptive transfer of TILs, TILs are extracted from tumor tissue and antigen specific T cells undergo clonal expansion *ex vivo* in

presence of IL-2 and then will be returned to patient's body. In the latter forms of T cell therapy, after isolation of peripheral T cells, T cells are subjected to different type of genetic modifications for expression of second TCR or co-stimulatory molecules or a chimeric receptor (partly constituted of tumor antigen specific recognition and CD3/co-stimulatory molecule trans-membrane and cytoplasmic domains). Despite that adoptive T cell therapy improves response rates by up to 30% in some patients, this strategy is not effective against all type of cancers. The emergence of neoantigens in tumor cells, the inability of engineered T cells to recognize post-translationally modified antigens, and downregulation of major histocompatibility complex (MHC) on immune cells in the tumor microenvironment make T cell therapy a fragile strategy. Other drawbacks in T cell therapy that could be mentioned are difficulty in delivering of expanded T cells into malignant tissues and highly expensive strategy (21)(22). In addition, trafficking of transferred T cells into healthy tissues not only increases chance of autoimmunity but also might interfere with other immune system functions. Last but not least, recruitment of T cells into the tumor tissue does not guarantee effective responses since the recruited cells are under the influence of tumor microenvironment (TME) cues(23). The immunosuppressive environment of tumor tissue not only promotes tumor progression but also impairs immune responses. Therefore, cell therapy in cancer is inevitably limited to a few types of cancer like hematologic malignancies(24)(25). The major clinical gains in solid tumor immunotherapy were achieved when ICIs introduced in the mid-1990s. ICIs are monoclonal antibodies that block checkpoint proteins on T cells or their cognate ligands on the surface of other immune subsets and tumor cells (26). Immune checkpoint proteins are a group of inhibitory and co-stimulatory molecules that modulate immune responses through ligand-receptor interactions. Inhibitory immune checkpoint proteins maintain self-tolerance and the duration of the immune response while co-stimulatory immune checkpoint proteins promote cell proliferation and activation of cytokine pathways. Under physiological condition, a balance between the activating and inhibitory functions of checkpoint proteins maintains immune homeostasis. However, in the context of cancer, immune cells (specifically tumor-associate immune cells) overexpress inhibitory checkpoint proteins on their surface. Overexpression of inhibitory checkpoint molecules on the surface of TILs and their cognate ligands on other cells in TME results in contact-dependent immunosuppression in T cells. Therefore, targeting co-inhibitory molecules with ICIs disrupts inhibitory signals and enhances immune-mediated elimination of tumor cells (Figure 1). Although most of the characterized

checkpoint proteins in TME are expressed on T cells, it has been recently shown that a subset of myeloid population also express T-cell immunoglobulin and mucin-domain containing-3 (Tim-3) and Programmed cell death protein 1 (PD-1) (27). Therefore, ICIs not only target T cells in TME but also impact myeloid cells too. For instance, two monoclonal antibodies, ipilimumab and lambrolizumab, which block cytotoxic T-lymphocyte-associated protein 4 (CTLA-4) and PD-1 respectively, enhance response rates among metastatic melanoma patients and melanoma-bearing mice by unleashing both adaptive and innate immune responses (28)(29)(30). Furthermore, it has been shown that blocking V-domain Immunoglobulin Suppressor of T cell Activation (VISTA) augmented the ability of tumor-associated myeloid cells to produce immune-stimulatory cytokines(31). Like other immunotherapies, ICIs are not free from adverse effects. ICIs target immune cells regardless of their locations in the body. Therefore, immunotherapy with ICIs might induce chronic or acute hyper-immunity in cancer patients which leads to immune-related adverse events in the long-term(32). Although ICIs have saved many lives and improved survival rates in cancer patients, it is worth to mention a very limited number of eligible patients (12-25%) for ICIs immunotherapy respond well to the treatment(33)(34).

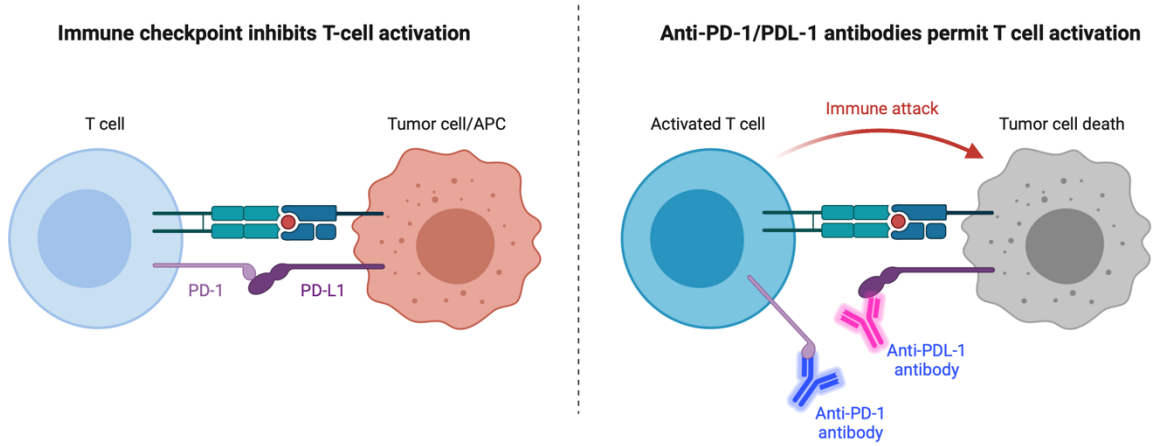

Fig 1 - Immune checkpoints are regulators of the immune system. Checkpoint proteins, such as PD-L1 on tumor cells/APCs and PD-1 on T cells, regulates T cell activation. The binding of PD-L1 to PD-1 prevents T cells from killing tumor cells (left panel). Blocking the binding of PD-L1 to PD-1 with an immune checkpoint inhibitor (anti-PD-L1 or anti-PD-1) allows the T cells to kill tumor cells (right panel).

During the past decade, the field of immuno-oncology has dramatically advanced. Different types of immunotherapy have been examined to enhance durable immune responses in solid tumors and many clinical trials have been conducted to measure the efficacy of therapies. However, the complexity of immune mechanisms, immunotoxicity of some medications and variability of tumor biology in patients, prevent wide application of immunotherapies in the clinics. Therefore, further studies are needed to understand the regulatory mechanisms involved in TME immunity, overcome potential barriers in immunotherapy and improve safety and efficacy of current therapies (35)(36). The TME is a highly heterogeneous environment consisting of different cell types including tumor cells, stromal cells and immune cells and non-cellular components like extracellular matrix structural proteins, and secreted cellular mediators. In such environment, immune cells constantly interact with other cells and influence overall structure of TME. Although immune subsets like CTLs and natural killer cells (NKs) are considered as the main warriors in this environment, the effector functions of these cells can be directly influenced by functionality of other immune subsets such as tumor-associated myeloid cells (37)(38). Recent studies have emphasized the crucial role of tumor-associated macrophages and neutrophils in cancer immunotherapy (39). For many years researcher focused on antigen presentation properties of myeloid cells in TME, though it is now clear that this population could actively participate in progression of cancer too. For example, anti-inflammatory macrophages (M2) can modulate the TME milieu in the favor of tumor cells and myeloid-derived suppressor cells (MDSCs) actively supress immune responses in TME and promote tumorigenesis. (40).

Dectin-1

Targeting tumor-associated myeloid cells via pattern recognition receptors (PRRs) agonists is a novel strategy in cancer therapy. PRRs are germline-encoded sensors mainly expressed by innate immune cells like dendritic cells, macrophages, neutrophils, and NK cells and classified into two groups: membrane-bound and cytoplasmic PRRs(41). Depending on specificity and localization of these molecules, they recognize variety of pathogen-associated molecular patterns (PAMPs) as well as endogenous damage-associated molecular patterns (DAMPs). Although, PRRs are integral components of innate immunity in maintaining tissue homeostasis and responding to intruding pathogens, their essential role in TME is inevitable(42)(43). These molecules are expressed by different cell types in TME, hence, targeting them can result in activation of signaling pathways

and release of inflammatory cytokines(44). Therefore, using PRRs agonist alone or in combination of other types of immunotherapy like ICIs is an ideal strategy for boosting anti-tumor immune responses (45)(44)(46). On the other hand, chronic activation of PRRs due to release loads of DAMPs in TME can promote tumorigenesis(47)(48). For many years, PRRs were represented by Toll-like receptors (TLRs) and studies on the roles of PRRs in cancer therapy were mainly limited to a few members of this family (49)(50). However, recent studies have shown that the role of PRRs in tumor immunity is not limited to TLRs but also extends to other PRR families like membrane-bound C-type lectin receptors (CLRs)(44). CLRs are a large family of soluble and transmembrane proteins that comprise a minimum of one conserved carbohydrate-recognition domain binding to glycan structures in a Ca^{2+} dependent manner(51). Among transmembrane proteins CLRs, Dendritic cell-associated C-type lectin-1 (Dectin-1), Dendritic cell-associated C-type lectin-2 (Dectin-2), Macrophage inducible Ca^{2+}-dependent lectin receptor (MINCLE) and Dendritic Cell-Specific Intercellular adhesion molecule-3-Grabbing Non-integrin (DC-SIGN) are well known molecules due to their ability to recognize carbohydrate structures like β-glucan structures, α-mannans and N-glycans (52). Although CLRs are mainly bind to carbohydrate structures, it has been shown that these molecules are also able to bind to non-carbohydrate structures such as protein and lipid ligands indicating the importance of their roles in immune system(53)(54)(55). Dectin-1 is a transmembrane CLR best known for its ability to recognize β-glucan-rich structures in fungal cell walls. (56). A full-length Dectin-1, also known as isomer A, comprises one extracellular C-type lectin-like domain, stalk region, a transmembrane domain and immunoreceptor tyrosine-based activation motif (ITAM)(57)(58). Following interaction with a cognate ligand, the ITAM motifs of Dectin-1 get phosphorylated by Src family kinases to create a docking site for spleen tyrosine kinase (Syk). Activation of Dectin-1 subsequently initiates two signaling pathways: Syk-dependent and Syk-independent pathways (Fig. 2)(59). In the former one, phosphorylated Syk activates Caspase recruitment domain-containing protein 9 (CARD9) and/or Mitogen-activated protein kinase (MAP) which ultimately lead to NF-κB activation, cytokine production, phagocytosis and respiratory burst(60)(61). However, in Syk-independent signaling pathway (non-canonical pathway), Dectin-1 activates Raf-1 kinase which subsequently enhances NF-κB activation. On the other hand, it was reported that suppressor of cytokine signaling protein 1 (SOCS1) is induced following stimulating Dectin-1 with depleted zymosan in murine bone marrow-derived macrophages. SOCS1 protein is a negative feedback inhibitor for type I and II

cytokine receptors which indirectly regulates the sensitivity of macrophages to interferon gamma (IFN-γ)(62)(63). Also, it is reported that Dectin-1 activation in macrophages and dendritic cells induces reactive oxygen species (ROS) through Syk-dependent pathway(60). Although low levels of ROS are essential for many cellular functionalities, overexpression of these molecules by myeloid cells in TME is detrimental(64). Overproduction of ROS in myeloid cells not only induce immunosuppressive phenotype in these cells but also promotes expression of PDL-1 on the surface of them in both human and mice(65). Furthermore, high concentration of ROS reduces antitumor function of T cells and increase T cell apoptosis. Therefore, activation of Dectin-1 in TME might result in activation of inflammatory responses or tolerogenic pathways.

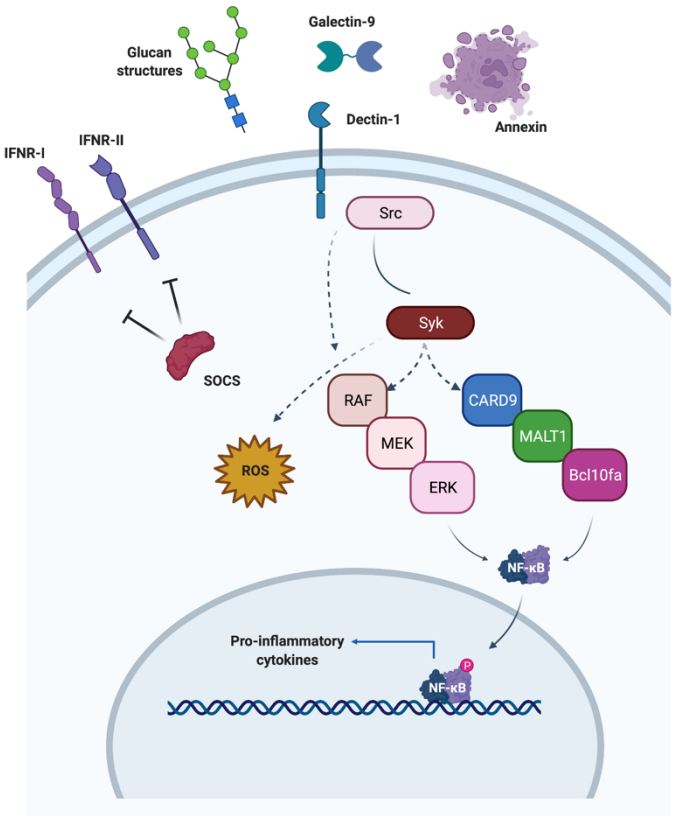

Fig- 2 Dectin-1 activates different signaling pathways. Dectin-1 mediates intracellular signaling through Syk-dependent and Syk-independent pathways. Src kinases phosphorylate tyrosine residues of ITAM in cytoplasmic tail of Dectin-1 and create site for Syk which pledges downstream signaling through molecules including CARD9 or MKK adaptive proteins which results in NF-κB activation and inflammatory cytokines production. Syk phosphorylation also induce ROS production.

It is worth to mention that Dectin-1 differentially interacts with β-glucan structures, proteins, chitin, mannans and lipids on pathogens and tumor cells(66). Therefore, one can speculate that different Dectin-1 ligands might induce different responses in myeloid cells. Many studies demonstrated that stimulating Dectin-1 by cognate agonists like curdlan, zymosan and yeast-derived β-glucans boost anti-tumor immune responses. For instance, NK cell-dependent tumor cell clearance relies on Dectin-1 interaction with N-glycan structures of tumor cells through activation of the Interferon Regulatory Factor 5 (IRF5) transcription factor and NK-mediated tumor cell killing(67). Another study also reported that activation of CARD9 axis following Dectin-1 and β-glucans ligation resulted in macrophage metabolic reprograming and M1 polarization of tumor associated-macrophages(68). However, because of availability of various ligands in TME, it is also speculated that Dectin-1 activation might result in different outcomes under pathological conditions(69). For example, it is reported that activation of Dectin-1 and mannose receptor (CD206) in TME are correlated with tumor progression (70)(71)(54). Recently, Daley et al described that Dectin-1 ligation with Galecin-9 (Gal-9) in TME accelerated the progression of tumor while blocking Dectin-1 downstream signal was a protective strategy in mice model of pancreatic ductal adenocarcinoma (PDA) (54). Furthermore, Bode et al showed that Dectin-1 binding to annexins molecules (annexin A1, A5, and A13) exposed by apoptotic cells induced tolerogenic responses via overproduction of reactive oxygen species (ROS) in dendritic cells (71).

Rationale

Despite that activation of Dectin-1 signalling pathways in fungal infections lead to the induction of inflammatory responses and pathogen removal, functional consequences of Dectin-1 activation in TME remains poorly defined and controversial. Availability and diverse affinity of Dectin-1 ligands in the complex environment of the tumors makes it difficult to predict the outcome of Dectin-1 signaling. Furthermore, Dectin-1 is expressed by different immune subset in TME which each of these subsets exert different functionality. Finally, the immunogenicity of TME is a determining factor in response to immunotherapy. Therefore, characterising different Dectin-1 expressing immune cells in different tumor models provides insights into the mechanisms of protection/suppression mediated by these cells in TME. Furthermore, investigating Dectin-1 expressing immune subsets in TME lets us know whether this molecule is a valuable predictive and/or prognostic biomarker in cancer. Finally, targeting (blocking or stimulating) Dectin-1 alone

or in combination with another immunotherapy like an immune checkpoint inhibitor helps us to know whether Dectin-1 is a potential target for immunotherapy or not.

Research questions and hypothesis

To have a better understanding of roles of Dectin-1 in TME, I asked what are the characteristics of Dectin-1 expressing cells in immunogenic and non-immunogenic tumors and how can I improve immunotherapy by targeting immune cells by using a Dectin-1^{+} agonist and an immune checkpoint inhibitor? I first hypothesized that Dectin-1 expressing immune cells in non-immunogenic tumor models (tumors with insufficient antigens and impaired T cell priming) like B16-F10 melanoma probably display immunosuppressive phenotypes while they might be protective in immunogenic tumor models like CT26 colorectal cancer. Since targeting Dectin-1 alone might result in tolerogenic signals in TME, I also hypothesized that activation of Dectin-1 alongside blockade of one co-inhibitory checkpoint molecule could improve immune responses (Fig. 3). The goal of this research project was to examine Dectin-1 as a potential predictive biomarker and target for immunotherapy in cancer. To test my hypothesis and address the questions, I sought to 1) identify myeloid, lymphoid and non-immune populations expressing Dectin-1 in immunogenic and non-immunogenic tumor microenvironments, 2) determine the immune profile of Dectin-1^{+}/Dectin-1^{-} expressing myeloid and lymphoid cells in an immunogenic and non-immunogenic tumor model, and 3) determine if the combination of Dectin-1 agonist (curdlan) and α–VISTA monoclonal antibody has a synergistic effect in anti-tumor immune responses.

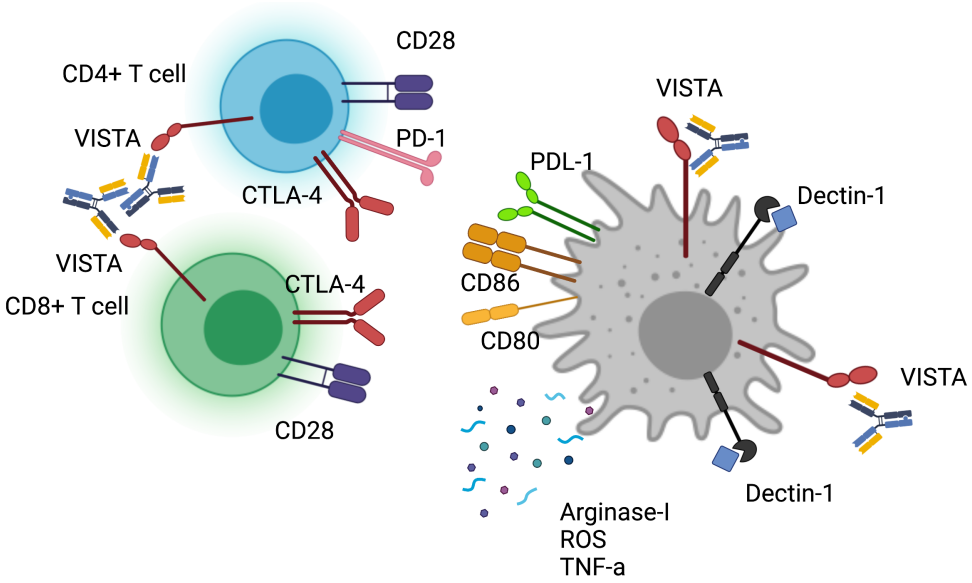

Fig 3. Targeting adaptive and innate immune cells in TME improves anti-tumor immunity. I hypothesized that targeting myeloid cells by Curdlan (Dectin-1 agonist) and α-VISTA monoclonal antibody and lymphocyte by α-VISTA monoclonal antibody improve immune response in cancer patients.

In the present study, I investigated the distribution of Dectin-1 expression in the TME, spleen and peripheral blood of two tumor models: B16-F10 melanoma and CT26 colorectal cancer. Confirming the previous studies, I determined that overall expression of Dectin-1 highly upregulated in tumor cells and myeloid subsets in the TME of both B16-F10 melanoma and CT26 colorectal tumor models. However, it was more remarkable in B16-F10 melanoma model. I also characterized the myeloid population in tumor tissue and spleen of tumor-bearing mice by comparing effector functions of Dectin-1^{+} versus Dectin-1^{-} myeloid cells. My findings showed that Dectin-1^{+} myeloid cells not only expressed more inhibitory checkpoint molecules (VISTA, PDL-1 and PDL-2) on their surface in TME but also expressed significant amounts of immunosuppressive molecules. Given a significant co-expression of inhibitory checkpoint molecules on myeloid cells, I also investigated myeloid cells for any co-localization of Dectin-1 with VISTA and PDL-1 on. Finally, I investigated the role of VISTA in Dectin-1 knock out mice and similarly analyzed targeting Dectin-1 with and without an agonist in the B16-F10 model. Taken together, my results imply that Dectin-1 stimulation could be considered in combination with other ICIs to enhance both arms of immune systems against cancer.

Methods and Materials

Ethics statement

All animal studies were carried out according to the Guide for the Care and Use of Laboratory Animals of the Canadian Council for Animal Care (CCAC). The experimental protocol was approved by the Animal ethics boards at the University of Alberta (Protocol # AUP00002737).

Animals

Male and female BALB/c and C57BL/6 mice were purchased from the Charles River Laboratory. VISTA$^{-/-}$ mice in C57BL6/J background were kindly provided by Dr. Roy A. Fava. Dectin-1 knockout (also known as clec7a$^{-/-}$) mice were purchased from the Jackson Laboratory. All animals were housed under controlled environmental conditions (25°C and a 12-hour light/dark cycle, 5 mice per cage) within the animal care facility at the University of Alberta. Iused 6–8 weeks age and sex-matched mice in all my experiments.

Cell lines and cell cultures

Frozen B16-F10 melanoma (Cat# CRL-6475™) and CT26 (Cat# CRL-2638™) colorectal tumor cells obtained from American Type Culture Collection (ATCC). Frozen cells were tawed and washed in complete media (RPMI 1640 Medium (with L-glutamine and sodium bicarbonate, liquid, sterile-filtered, Cat# R8758) supplemented with 1% penicillin/streptomycin (Sigma, Cat#P0781-100ML) and 10% heat-inactivated FBS (Sigma, Cat# F1051-100ML)) at approximately 125 x g for 5 to 10 minutes. Rinsed cells then dispensed into 25 cm^2 culture flasks and incubated at 37°C in 5% CO_2 incubator. When cells reached 75% confluency, culture media were removed, and culture flask rinsed with Dulbecco′s Phosphate Buffered Saline (PBS, Cat# D8537-100ML) to remove all traces of serum that contains trypsin inhibitor. Next, 2.0 ml of Trypsin-EDTA, 0.05% (ThermoFisher, Cat# 25300054) solution was added to flasks and cells were observed under an inverted microscope until cell layer is dispersed (5-7 minutes). To neutralize trypsin, 8.0 mL of complete media was added to culture flasks. Expanded cells then wash with complete media and appropriate aliquots of the cell suspension were added to new culture flasks. Growth media were exchanged every 2 to 3 days in subcultures. For tumor inoculation, appropriate number of cells diluted in 100 µl of PBS. To store expanded tumor cells,

cells were dissolved in 90% FBS and 10% dimethyl sulfoxide (DMSO) solution and then split in 2 ml cryovials. Cryovials then were put in cell freezing chamber and transferred to -80 freezer for overnight. Frozen cryovials were transferred to the liquid N2 tank next day.

Animal cancer models

Animals were gently transferred into pre-oxygenated sealed knock down chamber by the tail. O_2 flow meter was set to 1000 mls/min for the O^2 flow rate. The isoflurane gauge was turned on. Isoflurane level was increased slowly to in order to provide a smooth induction (Start off with 0.5% and then increased by 0.5% increments every few breaths). Once consciousness lost (the mouse remains recumbent and cannot right itself), the animal wase removed from the knockdown chamber and transfer to the nose cone and Bain circuit. The isoflurane and the oxygen then were turned back on to 2% and flow to 500 ml/min respectively. The depth of anesthesia was checked by by checking pedal or toe pinch reflex on all four paws and vital signs were regularly monitored. The left flank was shaved with clipper and area was sterile by alcoholic pad. When the procedure has been completed, the Isoflurane was turned off and after 10 seconds the animal transferred to recovery chamber. To generate tumors, expanded tumor cells were injected subcutaneously into the left flank of mice under complete isoflurane inhalation anesthesia (Mouse S-1 Isoflurane Anesthesia and Monitoring in the Mouse SOP, HSLAS, University of Alberta). Cell numbers were determined based on previous studies (B16-F10 = 1×10^5 in 100µ PBS per mouse, CT26 = 1×10^5 in 100µ PBS per mouse)(72)(73). Five to seven days after injection, palpable tumors formed. For immunotherapy experiments, animals received intraperitoneally (i.p.) 200 µl of curdlan (10-15 mg/Kg, Sigma-Aldrich curdlan, Cat# C7821-5G) solution (curdlan was dissolved in 0.1N NaOH (4gr NaOH in 1 liter of distilled water) or 200 µl of anti-VISTA antibody (300 µg per mouse , Bio X Cell 13F3, Cat# BE0310) alone or in combination(74)(75). In the case of anti-VISTA immunotherapy, the antibody was first injected on day six and then administrated every three days for three times. In the case of curdlan immunotherapy, curdlan was first injected on day one and then administrated every two days for five times. Animals were daily monitored until day 16 and then euthanized via carbon dioxide chamber. Tumor tissues, spleens and peripheral bloods were collected from each mouse immediately. Tumor size was measured at the end of each experiment and the tumor volume was calculated according to the length x $width^2/2$ formula, where length represents the largest diameter of tumor and width represents the perpendicular tumor diameter.

Tissue collection and processing

To obtain a single-cell suspension, spleen were ground between sterile frosted glass slides in 7 ml of 1× RBC lysis buffer (8.3 gm/l NH4Cl in 0.01 M Tris–HCl buffer of pH 7.5) per spleen and then filtered through 40 or 70 micron nylon mesh (Fisherbrand™ Sterile Cell Strainer, Cat#352360 and 352340) as reported elsewhere(76). Then cells were resuspended in complete media (RPMI 1640 Medium (with L-glutamine and sodium bicarbonate, liquid, sterile-filtered, Cat# R8758) supplemented with 1% penicillin/streptomycin (Sigma, Cat#P0781-100ML) and 10% heat-inactivated FBS (Sigma, Cat# F1051-100ML)). Tumor tissues were dissected aseptically, washed two times with Hanks' Balanced Salt Solution (Modified, with sodium bicarbonate, without calcium chloride and magnesium sulfate, liquid, sterile-filtered, Sigma Cat# H9394-1L), cut in small pieces in lysis buffer contained 20U/ml DNaseI (FisherScientific, Cat#PI90083) and 200 U/ml Collagenase type IV (ThermoFisher, Cat#17104019). Tumor samples were then transferred to 15 ml conical tubes and incubated for 25 minutes at 37° C inside a shaking incubator with 500rpm. Samples then were washed with complete medium, filtered through 70 and 40 μm nylon mesh and resuspended in complete media. To exclude tumor cells and debris from immune cells, samples were centrifuged on Ficoll®-Paque PREMIUM 1.084 (Sigma, Cat#GE17-5446-02) at 2000rpm for 20 minutes in the break-off mode. Isolated mononuclear cells then washed with complete media and prepared for further experiments. Blood samples were taken from the heart via Cardiac puncture technique following euthanasia by CO_2 chamber. After death confirmation, Iperformed the mouse cardiac puncture and 0.5 to 0.7 ml of blood collected in K3-EDTA (1.6 mg/ml blood) coated microtubes via 23G needles. Blood samples next lysed by RBC lysis buffer for 10 minutes and then washed by PBS and prepared for flowcytometry staining.

Flow cytometry, image cytometry and cell sorting

LIVE/DEAD Fixable Dead Cell Stain kit (Life Technologies, Cat# L34960) used to distinguish live cells from dead cells based on cell membrane integrity and access to available amines. 1-3 × 10^6 cells transferred to U bottom 96 -well plate and then stained with 200 μl of dye solution for 30 minutes at 4° C and then washed with PBS. Dead cells were excluded later from live cells during data analysis. The fluorochrome-conjugated antibodies were purchased from ThermoFisher Scientific, BD Biosciences, or BioLegend (Table 1). 1-3 × 10^6 cells from every samples were stained with antibody master mix in 96 -well plate and the incubated for 30 minutes at 4 ° C. Cells

next washed with Fluorescence-activated cell sorting (FACS) buffer (PBS with 2% FBS) and fixed with 4% paraformaldehyde (PFA) solution (PBS with 4% PFA). For intracellular staining, cells were permed and fixed with BD Cytofix/Cytoperm™ Fixation/Permeabilization Solution Kit (BD, Cat#BDB554714) in 96 -well plate according to manufacturer protocol and then stained with intracellular antibodies diluted in Perm/Wash buffer (BD, Cat#BDB554714). Stained cells then rinsed with Perm/Wash buffer and fixed in 4% PFA. Fixed cells were transferred to flow cytometry tubes and acquired on a Fortessa-X20 or LSR Fortessa-SORP flow cytometer (BD Biosciences) or Amnis® ImageStream®X Mk II Imaging Flow Cytometer. Data were analyzed using Flow Jo software (BD, version 10.7) and IDEAS (Amnis Corporation, version 6.0). For cell sorting, stained cells were resuspended in FACS buffer (PBS with 2% FBS) and sorting was performed by gating on $CD45^+$ live cells with SONY MA900 Multi-Application Cell Sorter. The production of intracellular reactive oxygen species (ROS) was measured using 2',7'-dichlorofluorescein diacetate (Sigma, Cat# D6883-50MG). The ROS staining was conducted according to the manufacturing protocol and detected by flow cytometry.

Table 3. The list of used antibodies and reagents in this study.

Antibodies/Reagents	Clone	Fluorophore	Catalog Number	Vendor
Monoclonal anti-mouse Arginase-1	IC5868A	APC	IC5868A	R&D
Monoclonal anti-mouse CD11b	M1/70	PE-Cy7	552850	BD Bioscience
Monoclonal anti-mouse CD11b	M1/70	PerCPCy5.5	550993	BD Bioscience
Monoclonal anti-mouse CD152 (CTLA-4)	UC10-4F10-11	APC	564331	BD Bioscience
Monoclonal anti-mouse CD206	MR6F3	PerCP-e710	46-2061-80	Invitrogen
Monoclonal anti-mouse CD223 (LAG-3)	C9B7W	BV786	740959	BD Bioscience
Monoclonal anti-mouse CD26	H194-112	BV650	740474	BD Bioscience
Monoclonal anti-mouse CD273 (PDL2)	TY25	APC	560086	BD Bioscience
Monoclonal anti-mouse CD274 (PDL1)	MIH5	PE	558091	BD Bioscience
Monoclonal anti-mouse CD3	17A2	APC-Cy7	560590	BD Bioscience
Monoclonal anti-mouse CD39	24DMS1	PE-Cy7	25-0391-82	eBioscience
Monoclonal anti-mouse CD3e	17A2	BV421	56-0032-80	eBioscience
Monoclonal anti-mouse CD4	GK1.5	BV786	563331	BD Bioscience
Monoclonal anti-mouse CD44	IM7	BV421	563970	BD Bioscience
Monoclonal anti-mouse CD45	30-F11	PE-Cy7	25045182	Invitrogen

Antibodies/Reagents	Clone	Fluorophore	Catalog Number	Vendor
Monoclonal anti-mouse CD45	30-F11	PE	553081	BD Bioscience
Monoclonal anti-mouse CD45	30-F11	PerCPCy5.5	550994	BD Bioscience
Monoclonal anti-mouse CD49d	R1-2	FITC	11-0492-82	Invitrogen
Monoclonal anti-mouse CD62L	MEL-14	PerCPCy5.5	560513	BD Bioscience
Monoclonal anti-mouse CD73	TY/23	v450	561544	BD Bioscience
Monoclonal anti-mouse CD8	53-6.7	A700	56-0081-82	eBioscience
Monoclonal anti-mouse CD80	16-10A1	e450	48-0801-82	eBioscience
Monoclonal anti-mouse CD86	GL1	PE	12-0862-82	eBioscience
Monoclonal anti-mouse Dectin-1 (CD369)	bg1fpj	PE-Cy7	25-5859-80	Invitrogen
Monoclonal anti-mouse Dectin-1 (CD369)	1,50E^{+}03	FITC	MA5-16479	Invitrogen
Monoclonal anti-mouse F4/80	6F12	BV421	563900	BD Bioscience
Monoclonal anti-mouse Gal-9	RG9-35	PerCPCy5.5	136112	BioLegend
Monoclonal anti-mouse GATA3	L50-823	BUV395	565448	BD Bioscience
Monoclonal anti-mouse Granzyme B	NGZB	e450	48-8898-82	Invitrogen
Monoclonal anti-mouse I-A/I-E (MHC-II)	M5/114	PerCPCy5.5	562363	BD Bioscience
Monoclonal anti-mouse IFN-γ	XMG1.2	PE-Cy7	61-7311-82	eBioscience
Monoclonal anti-mouse IL-10	C17.8	PE	12-7101-82	eBioscience
Monoclonal anti-mouse IL12/IL-23p40	C17.8	e660	50-7123-82	eBioscience
Monoclonal anti-mouse Ki67	SolA15	e450	48-5698-82	eBioscience
Monoclonal anti-mouse Ly/6C	HK1.4	PE	12-5932-80	eBioscience
Monoclonal anti-mouse Ly/6G	1A8	Alexa 700	561236	BD Bioscience
Monoclonal anti-mouse NK1.1 (CD161)	PK136	PE	12-5941-82	eBioscience
Monoclonal anti-mouse Perforin	S16009B	PE	154405	BioLegend
Monoclonal anti-mouse RORγt	Q31-378	BV786	564723	BD Bioscience
Monoclonal anti-mouse Tbet	O4-46	V450	561312	BD Bioscience
Monoclonal anti-mouse Tim3 (CD366)	5D12	BUV395	747620	BD Bioscience
Monoclonal anti-mouse TNF-α	MP6-XT22	v450	560655	BD Bioscience
Monoclonal anti-mouse VISTA	MIH64	PE	566269	BD Bioscience
InVivoMAb anti-mouse VISTA	13F3	N/A	BE0310	BioXCell
Fluorometric Intracellular Ros	N/A	FITC	MAK144-1KT	Sigma Aldrich

Gene expression assay

Isolated cells from tumor tissue and spleen were subjected to total RNA extraction in TRIZOL reagent (Invitrogen, Cat# 15596026). Briefly, 300 µl of TRIzolTM reagent was added to each sample (5– 10 × 10^6 cells) in 2ml microtubes. Lysed cells stored in -80 freezer for further

experiments. RNeasy kit (Qiagen, Cat# 74004) used for purification of total RNA from cells based on RNeasy spin technology column according to the manufacturer protocol. A Nano-Drop ND-1000 Spectrophotometer (NanoDrop Technologies, Wilmington, DE, USA) was used to check the quantity and quality of RNA in 1µl of samples. Only high-quality samples with A260/A280 ratios between 1.8 and 2.2 and A260/A230 ratios >1.7 were used for cDNA generation. To synthesize first-strand cDNA, at least 500 ng of the isolated RNA was reverse transcribed using a QuantiTect Reverse Transcription kit (Qiagen, Cat# 205311) according to the manufacturer instruction. Generated cDNA used/stored for further assessments. Lyophilized mix of forward and reverse primers for Dectin-1 (QuantiTect Primer Assay Kit, Cat# 249900) and Glyceraldehyde phosphatidyl hydrogenase (GAPDH) (QuantiTect Primer Assay Kit, Cat# 249900) were obtained from Qiagen. The primers were reconstituted in TE, pH 8.0 (Invitrogen, Cat# AM9849) to give a 10x primer solution, which is then added to the master mix. The GAPDH was used as a housekeeping gene to normalize the cDNA levels. The negative controls contained water or reverse-transcription negative RNA instead of template DNA. Three technical repeats were prepared for each sample. Real-time PCR (RT-PCR) analysis of Dectin-1 gene expression was carried out using QuantiTect SYBR® Green PCR Kits (Qiagen, Cat# 204141) and the Bio- Rad CFX96 real-time cycler according to manufacturer protocols (Table 1 and 2). To calculate the relative gene expression the $2^{-\Delta\Delta Ct}$ method employed via Microsoft Excel (Microsoft Office, version 16.48) (77). First, the Ct values of technical replicates of each sample were averaged. Next, delta Ct (ΔCt) for each sample calculated by ΔCt = Ct (gene of interest) – Ct (housekeeping gene) formula. To calculate delta-delta Ct (ΔΔCt), the control average was first calculated by taking average of Ct values of the biological replicates of the control group (Spleen). The delta-delta Ct (ΔΔCt) was calculated by ΔΔCt = ΔCt (Tumor Tissue) – ΔCt (Spleen). Finally, to work out the fold gene expression, Fold gene expression = $2^{\wedge -(\Delta\Delta Ct)}$ formula was employed.

Table 1. Cycling conditions for two-step RT-qPCR (QiaGene, QuantiTect Primer Assays)

Step	Time	Temperature	Additional comments
UNG (optional) Carryover prevention	2 min	50°C	UNG will eliminate any dUMP-containing PCR products resulting from carryover contamination
PCR initial activation step	**15 min**	**95°C**	This step activates HotStarTaq DNA Polymerase
3-step cycling:			
Denaturation*	15 s	94°C	
Annealing	30 s	55°C	
Extension†	30 s	72°C	Perform fluorescence data collection
Number of cycles	35–40 cycles		The number of cycles depends on the amount of template cDNA and abundance of the target

* SmartCycler users can reduce denaturation time to 1 second to take advantage of cycling capacities.

† Due to software requirements, the fluorescence detection step must be at least 30 s with the ABI PRISM 7000, or 34 s with the Applied Biosystems® 7300 and 7500.

Table 2. Reaction setup for two-step RT-qPCR (QiaGene, QuantiTect Primer Assays)

Component	Volume/reaction	Final concentration
2x QuantiTect SYBR Green PCR Master Mix*	25 µl	1x
10x QuantiTect Primer Assay	5 µl	1x
Template cDNA (added at step 4)	Variable	≤100 ng/reaction
Optional: Uracil-N-glycosylase†	0.5 µl	0.5 units/reaction
RNase-free water	Variable	–
Total volume	**50 µl‡**	**–**

* Provides a final concentration of 2.5 mM $MgCl_2$.

† Supplied with the QuantiTect SYBR Green PCR +UNG Kit.

‡ If using a total volume other than 50 µl, adjust the amounts of the master mix and the primer assay so that their final concentrations remain 1x, but continue to use 0.5 units of UNG and ≤100 ng of template cDNA.

Immunofluorescence (IF) staining

Following tumor dissection, tumor tissues were rinsed with PBS and fixed in 4% PFA solution in 50 ml conical tubes overnight at room temperature. Fixed tissues were subjected to sectioning at the University of Alberta HistoCore Center. Following preparation of paraffin-embedded samples, slides were checked under the light microscope and high-quality ones were deparaffinized by washing twice in Xylene Cyanol FF (Sigma-Aldrich, Cat# X4126-10G) for 10 minutes, twice in 100 % ethanol alcohol (EtOH) for 10 minutes, once in 95 % EtOH for 5 minutes, once in 70 % EtOH for 5 minutes, and finally for 5 minutes wash in H_2O. For antigen retrieval, slides were incubated in pre-warmed Citrate Buffer (0.1 M, pH 6.0) for 10 minutes in a water bath at 92°C. Deparaffinized slides were removed and allowed to cool at room temperature and then washed three times with 1x PBS in 5 minutes intervals. To minimize non-specific binding, slides were incubated in 10 % donkey serum in 0.1% Phosphate-Buffered Saline Tween® (PBST) at room temperature for 1 hour and washed three times with 1x PBS in 5 minutes intervals. To stain CD11b and Dectin-1 in tumor tissue, slides were incubated in 100 µL of Rabbit/IgG anti-mouse CD11b

polyclonal antibody (1:200 dilution, 0.5-1 µg/mL, InvitroGen, Cat#PA5-79532) and/or 100 µL of Rat/IgG2b anti-mouse Dectin-1 antibody (1:200, 1 µg/mL, InvitroGen, Cat#MA5-16477) overnight in a moist chamber at 4°C. For the negative control, samples were incubated with 100 µL PBS overnight in a moist chamber at 4°C. The next day slides were washed three times with PBS in 5 minutes intervals. Then, the slides were stained in the dark, either 100 µL of Donkey anti-Rabbit IgG Alexa Fluor Plus 488 (1:1000 dilution, 1-10 µg/mL, Invitrogen Cat#A32790) and/or Goat anti-Rat IgG Alexa Fluor Plus 555 (1:1000 dilution, 1-10 µg/mL, Invitrogen A48263) secondary antibodies. The slides were incubated 1 hour in the dark at room temperature and then washed three times with PBS for 5 minutes each wash. To visualize nuclear DNA in fixed tissues, slides were then incubated with 100 µL of blue DAPI (100 nM, Invitrogen D1306) for 10 minutes and washed three times with 1x PBS in 5 minutes intervals. To protect fluorescent dyes from fading, a drop of ProLong™ Gold Antifade Mountant (Invitrogen, Cat#P36934) was added to each sample before coverslips were placed. The hematoxylin and eosin staining was conducted using H&E Staining Kit (abcam, ab245880). Images were acquired on an Olympus IX73 microscope using 20X and 40X objectives.

Statistical analysis

A two-sample t-test, assuming equal variances, was applied with an alpha of 0.05 to determine if two groups were different from each other. Multiple comparisons between independent experimental immunotherapy groups (>2) were conducted by Kruskal–Wallis one-way analysis of variance followed by Dunn's multiple comparison correction in GraphPad Prism 9.2.0 (283). Due to presence of outliers among samples (an important assumptions for Pearson correlation), correlation between frequency of $CD45^+$ Dectin-1^+ cells and T cell subsets in tumor tissue was calculated by nonparametric spearmen correlation analysis in GraphPad Prism 9.2.0. Results are presented as mean ± standard error of the mean (SEM) on plots. P-value < 0.05 was considered as statistically significant.

Results

Dectin-1 is strongly expressed in a non-immunogenic tumor

Although some studies have shown that targeting Dectin-1 in TME enhances anti-tumor immune response(67)(68)(75), others have indicated that Dectin-1 expression in TME can aggravate tumor growth by switching M1 macrophages to M2 phenotype (78)(54). To better understand the role of Dectin-1 in tumor immunogenicity, I investigated the frequency of Dectin-1^+ immune cells in the tumor tissue, spleen, and peripheral blood of B16-F10 melanoma and CT26 colorectal tumor models (Fig 4). My analysis revealed that the TME in both tumor models had significantly higher Dectin-1^+ $CD45^+$ immune cells than the spleen and peripheral blood (Fig 4B and C). In particular, I found that $CD11b^+$ cells were the most prominent Dectin-1 expressing cells, and also a small portion of $CD3^+$ T cells expressed Dectin-1 in the TME (Fig. 4 B and D). Comparing two tumor models, I found that B16-F10 melanoma-bearing mice had a remarkably larger proportion of $CD45^+$Dectin-1^+ and $CD11b^+$Dectin-1^+ cells in their spleens and tumor tissues compared to the CT26 colorectal tumor model (Fig. 4 B and D). However, when $CD3^+$Dectin-1^+ T cells were analyzed, I only found a significantly higher abundance of these cells in the spleen of B16-F10 tumor-bearing mice than CT26 tumor-bearing mice (Fig. 4D). To confirm whether the intensity of Dectin-1 expression was increased in immune cells, I also compared the mean fluorescence intensity (MFI) of Dectin-1 among $CD45^+$ immune cells. Similarly, I observed that the intensity of Dectin-1 expression was greater on the surface of $CD45^+$ immune cells in TME compared to spleen and peripheral blood in both tumor models (Fig. 4E) Comparing the of MFI of Dectin-1 between two tumor models, I noted that the intensity of Dectin-1 was significantly higher in spleens and TMEs of the B16-F10 melanoma model than the CT26 colorectal cancer (Fig 4F). To test whether Dectin-1^+ myeloid cells originated from the periphery, I also compared the level expression of Dectin-1 in splenocytes and peripheral blood mononuclear cells (PBMCs) with TME. This analysis showed a significantly lower expression of Dectin-1 on total splenocytes and PBMCs compared to the TME resident cells in both tumor models (Fig. 4C and E). These observations imply that the upregulation of Dectin-1^+ expression is a product of the TME condition.

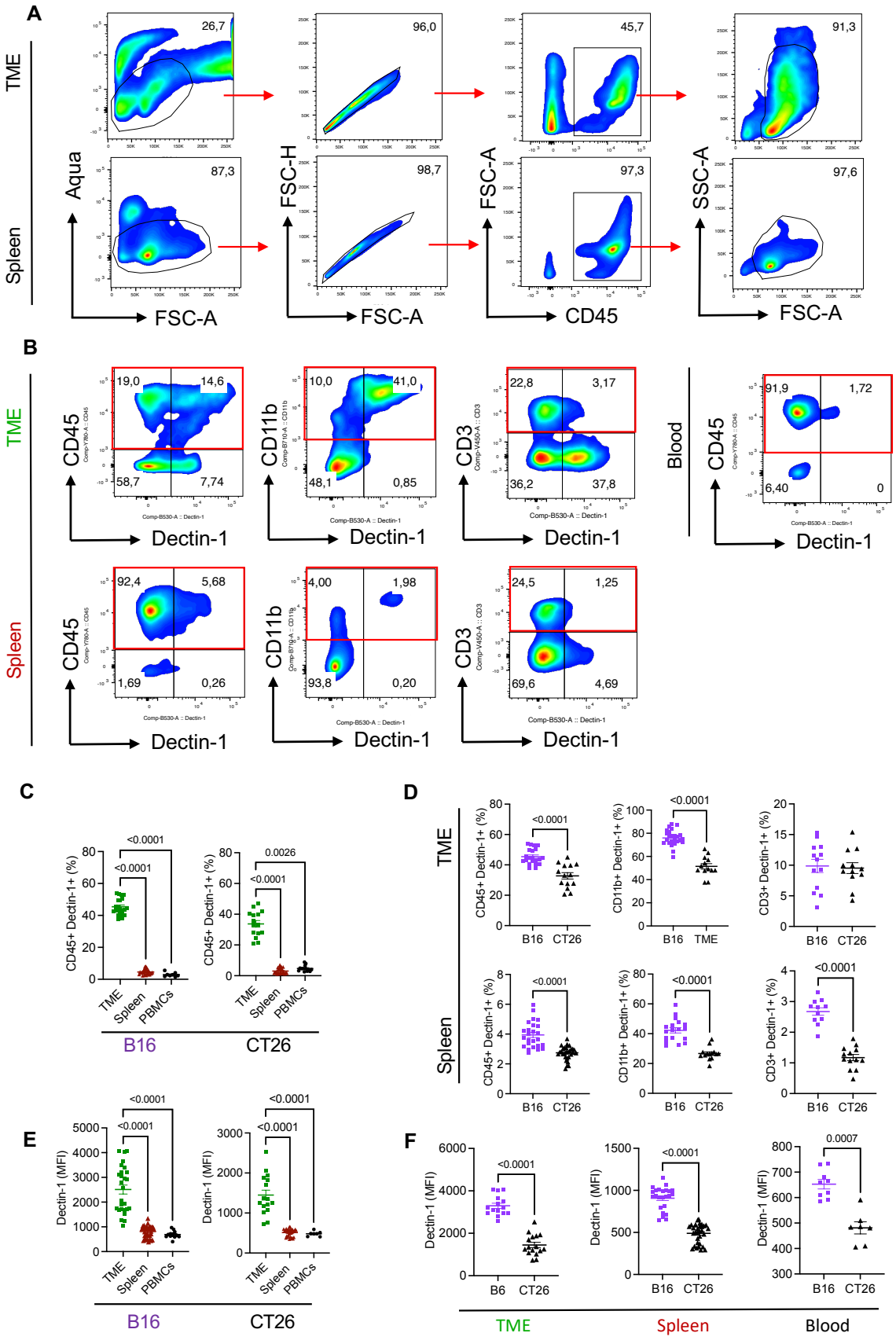
A
TME
Spleen
Aqua
FSC-A
26,7
87,3
FSC-H
FSC-A
96,0
98,7
FSC-A
CD45
45,7
97,3
SSC-A
FSC-A
91,3
97,6
B
TME
Spleen
CD45
CD11b
CD3
Blood
Dectin-1
19,0
14,6
58,7
7,74
10,0
41,0
48,1
0,85
22,8
3,17
36,2
37,8
91,9
1,72
6,40
0
92,4
5,68
1,69
0,26
4,00
1,98
93,8
0,20
24,5
1,25
69,6
4,69
C
CD45+ Dectin-1+ (%)
<0.0001
<0.0001
0.0026
<0.0001
TME
Spleen
PBMCs
B16
CT26
D
TME
Spleen
CD45+ Dectin-1+ (%)
CD11b+ Dectin-1+ (%)
CD3+ Dectin-1+ (%)
<0.0001
B16
CT26
TME
E
Dectin-1 (MFI)
<0.0001
<0.0001
<0.0001
<0.0001
TME
Spleen
PBMCs
B16
CT26
F
Dectin-1 (MFI)
<0.0001
<0.0001
0.0007
B6
B16
CT26
TME
Spleen
Blood

Fig 4. Dectin-1 is highly expressed on the surface immune cells in the tumor microenvironment (TME). (**A**) Representative flow cytometry plots showing the gating strategy for immune cells in the TME, spleen and peripheral blood. **(B**) Representative flow cytometry plots of the frequency of tumoral and splenic Dectin-1 expressing cells among $CD45^+$, $CD11b^+$, and $CD3^+$ T cells. (**C**) Cumulative data of percentages of $CD45^+$Dectin-1^+ in the TME, spleen and peripheral blood of B16-F10 and CT26 tumor-bearing mice. (**D**) Comparing the cumulative percentages of $CD45^+$Dectin-1^+, $CD11b^+$Dectin-1^+ and $CD3^+$Dectin-1^+ immune cells between CT26 and B16-F10 tumor models. (**E**) Cumulative data comparing the MFI of Dectin-1 in $CD45^+$ immune cells in the TME, spleen and peripheral blood of B16-F10 and CT26 tumor-bearing mice. (**F**) Cumulative data comparing the MFI of Dectin-1 in $CD45^+$ immune cells between B16-F10 and CT26 tumor models.

Parallel to the surface Dectin-1 protein expression, the level of celec7a gene (Dectin-1) expression was significantly higher in sorted $CD45^+$ immune cells from tumor tissues compared to their counterparts in the spleen (Fig. 5A). Of note and in agreement with protein levels, celec7a gene expression was significantly higher in sorted $CD45^+$cells from the TME of B16-F10 versus CT26 (Fig. 5A). To determine whether the frequency of Dectin-1 expressing cells influences the proportion of T cells in the TME, I analyzed the correlation between $CD45^+$Dectin-1^+ cells with total $CD3^+$, $CD4^+$ or $CD8^+$ T cells in the B16-F10 model that had significantly higher $CD45^+$Dectin-1^+ cells. I found a significant negative correlation between the frequency of $CD45^+$Dectin-1^+ with total $CD3^+$ and $CD8^+$ T cells but not $CD4^+$ T cells in the B16-F10 model (Fig. 5B). In contrast, I observed a significant but positive correlation between the frequency of $CD45^+$Dectin-1^+ cells and $CD3^+$ and $CD8^+$ T cells but not $CD4^+$ T cells in the CT26 tumor model (Fig. 5C). This may suggest different roles for Dectin-1 in an immunogenic versus non-immunogenic model as reported elsewhere(54)(78). Finally, I quantified the expression of Dectin-1 on $CD45^-$ cells in the TME that supposedly to be tumor cells. I found that majority of these cells expressed Dectin-1, however, $CD45^-$ Dectin-1 expressing cells were more abundant in B16-F10 versus CT26 tumors (Fig. 5D). Next, I assessed the expression of different co-inhibitory receptors/ligands, which showed these $CD45^-$ cells predominantly express PD-L1 but not PDL-2, VISTA and Gal-9 (Fig. 5E). Collectively, these results indicate higher Dectin-1 expressing cells in the TME and the non-immunogenic TME (B16-F10) comprised of more Dectin-1^+ immune cells in both the TME and spleen. Therefore, Dectin-1 might play an immunomodulatory role in the TME.

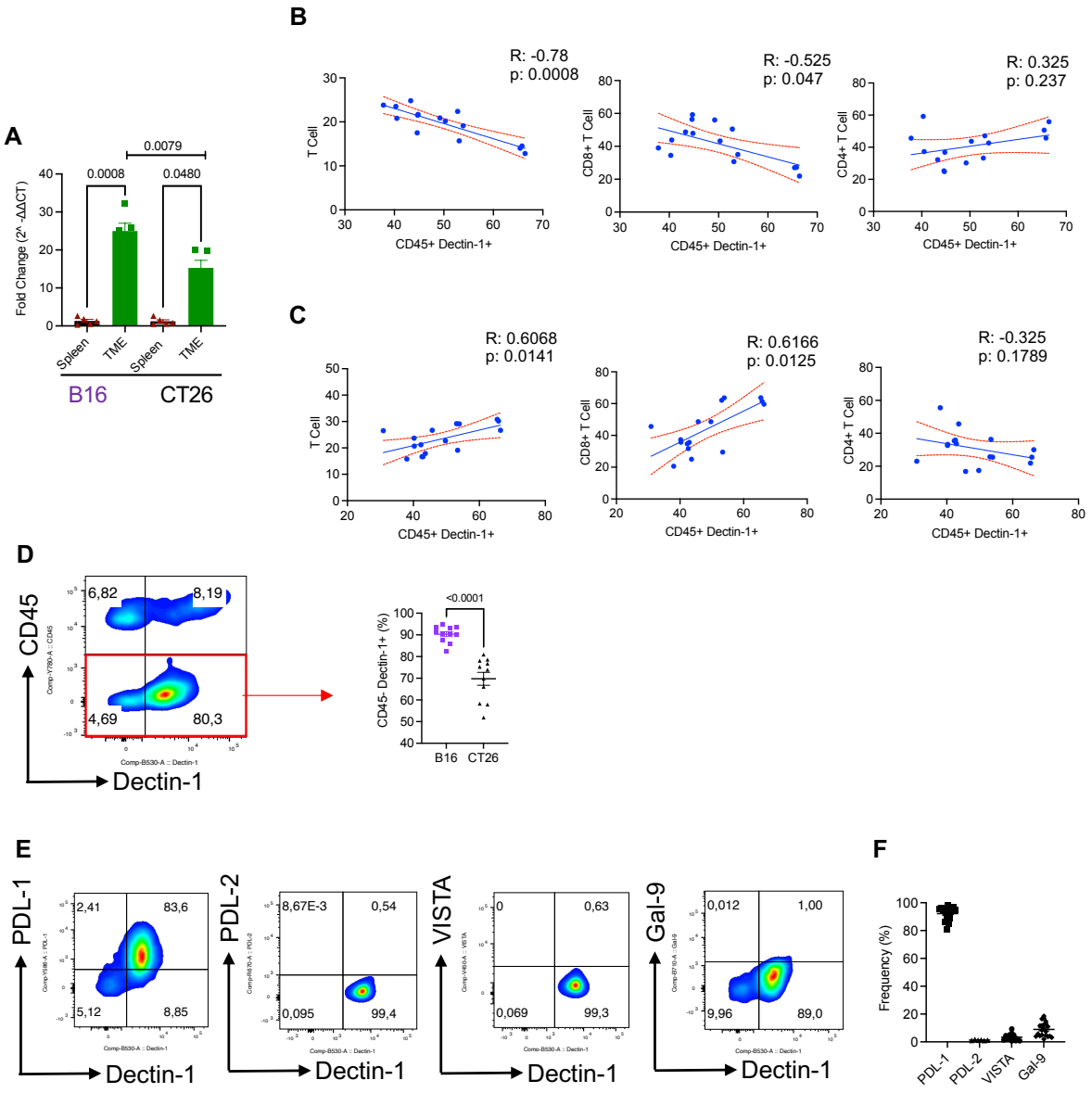

Fig 5. Dectin-1 is highly expressed on the surface of tumor cells in the tumor microenvironment (TME). (**A**) Cumulative data of fold change in mRNA expression for clec-7 in the TME and spleen of B16-F10 and CT26 tumor models. (**B**) Cumulative data of correlations between the frequency of total $CD45^{+}Dectin\text{-}1^{+}$ immune cells and $CD3^{+}$ T cells and $CD8^{+}$ T cells in the B16-F10 tumor model. (**C**) Cumulative data of correlations between the frequency of total $CD45^{+}Dectin\text{-}1^{+}$ immune cells and $CD3^{+}$ T cells and $CD8^{+}$ T cells in the CT26 tumor model. (**D**) Representative flow cytometry plot and cumulative data of percentage of $Dectin\text{-}1^{+}$ cells among live $CD45^{-}$ cells in the TME of B16-F10 and CT26 tumor models. (**E**) Representative flow cytometry plots of co-expression of Dectin-1 with PDL-1, PDL-2, VISTA and Gal-9 on $CD45^{-}$ live cells in the TME of the B16-F10 tumor model. (**F**) Cumulative data showing percentages of PDL-1, PDL-2, VISTA and Gal-9 on live $CD45^{-}$ cells in the TME of B16-F10 tumor model.

Tumor-associated myeloid cells express different levels of Dectin-1 in the TME

Unlike human myeloid cells, all subsets of myeloid cells in mice express different levels of Dectin-1(79). Therefore, I investigated the proportion of Dectin-1 expressing cells among different myeloid cells. I first characterized myeloid subsets including monocytes ($CD11b^{+}F4/80^{-}Ly6C^{low/mid}Ly6G^{-}$), macrophages ($CD11b^{+}F4/80^{+}$), M-MDSCs ($CD11b^{+}F4/80^{-}Lyc6^{High}Ly6G^{-}$) and G-MDSCs ($CD11b^{+}F4/80^{-}LyG6^{+}Ly6C^{-}$) in the TME and spleen of both tumor models (Fig. 6A). Ifound that in the B16-F10 model, the proportion of monocytes was significantly lower in the TME compared to their counterparts in the spleen (Fig. 6B). However, the proportion of M-MDSCs and G-MDSCs were significantly higher in the TME compared to their siblings in the spleen without any changes in the proportion of macrophages (Fig. 6B). Almost the same pattern was observed in the CT26 model except the proportion of macrophages was significantly higher in the TME compared to the spleen (Fig. 6B). Next, I evaluated the frequency of Dectin-1 expressing cells among different myeloid subsets. I observed significantly higher frequency of monocytes, tumor-associated macrophages and M-MDSCs expressing Dectin-1 in tumor tissues of B16-F10 mice compared to their siblings in the spleen (Fig.6C and D). Although the same pattern was noted for monocytes and macrophages in the CT26 model, the M-MDSC population didn't show any difference regarding the frequency of Dectin-1 expression cells between TME and spleen (Fig.6C and D). Interestingly, unlike M-MDSCs, the G-MDSC subpopulation had significantly lower proportion of Dectin-1 expressing cells in the TME compared to the spleen in both animal models (Fig.6C and D). Next, I compared the percentages of Dectin-1^{+} myeloid subsets in two tumor models, which showed only a significant increase in the frequency of Dectin-1^{+} G-MDSCs in the CT26 mouse model (both in the TME and spleen) without any difference for other myeloid subsets (Fig.6E).

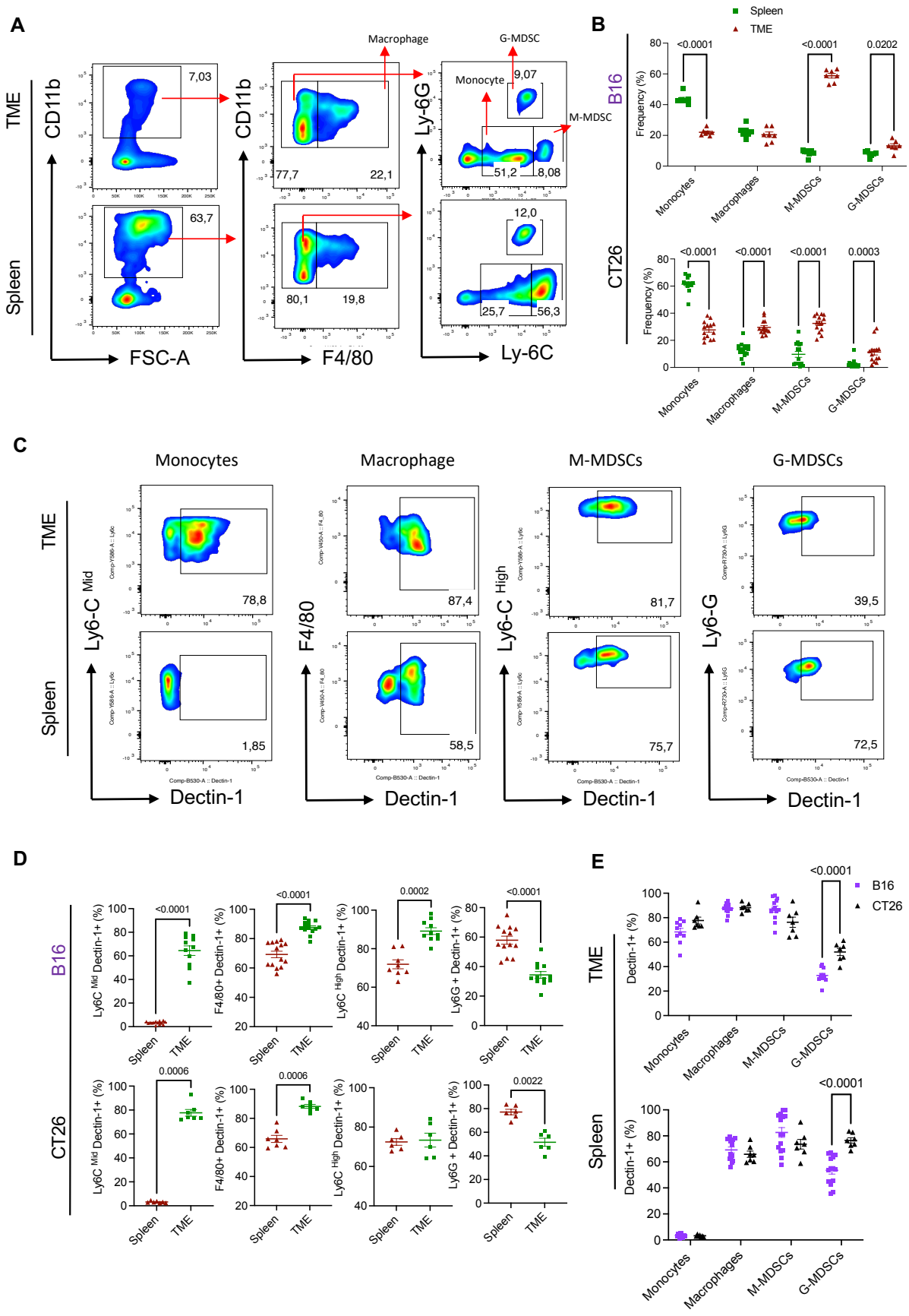
A
TME
Spleen
CD11b
FSC-A
7,03
63,7
F4/80
77,7
22,1
80,1
19,8
Macrophage
G-MDSC
Ly-6G
Ly-6C
Monocyte
9,07
M-MDSC
51,2
8,08
12,0
25,7
56,3
B
Spleen
TME
B16
CT26
Frequency (%)
<0.0001
0.0202
0.0003
Monocytes
Macrophages
M-MDSCs
G-MDSCs
C
Monocytes
Macrophage
M-MDSCs
G-MDSCs
Ly6-C Mid
Ly6-C High
Ly6-G
F4/80
Dectin-1
78,8
1,85
87,4
58,5
81,7
75,7
39,5
72,5
D
B16
CT26
Ly6C Mid Dectin-1+ (%)
F4/80+ Dectin-1+ (%)
Ly6C High Dectin-1+ (%)
Ly6G + Dectin-1+ (%)
Spleen
TME
<0.0001
0.0002
0.0006
0.0022
E
TME
Spleen
Dectin-1+ (%)
B16
CT26
<0.0001
Monocytes
Macrophages
M-MDSCs
G-MDSCs

Fig 6. Myeloid subsets express different levels of Dectin-1 in the tumor microenvironment (TME). (**A**) Representative flow cytometry plots of the gating strategy for myeloid subsets in the spleen and TME. (**B**) Cumulative data showing frequency of monocyte, macrophages, M-MDSCs and G-MDSCs in the spleen and TME of B16-F10 and CT26 tumor models. (**C**) Representative flow cytometry plots of percentages of Dectin-1 expressing monocytes, macrophages, M-MDSCs and G-MDSCs in the TME and spleen. (**D**) Cumulative data of percentages of Dectin-1^{+} monocytes (Ly6C^{Mid}), Dectin-1^{+} macrophages (F4/80^{+}), Dectin-1^{+} M-MDSCs (Lyc6^{High}) and Dectin-1^{+} G-MDSCs (LyG6^{+}) subsets in the TME and spleen of CT26 and B16-F10 tumor-bearing mice. (**E**) Cumulative data comparing B16-F10 and CT26 tumor models for percentages of Dectin-1 expressing monocytes, macrophages, M-MDSCs and G-MDSCs in the TME.

Since it has been reported that tumor-associated macrophages also express high levels of CD206, another reported pathogen recognizing CLR, in cancer(80), I measured the frequency of CD206 expressing macrophages in the TME of the melanoma-bearing mice. However, I did not detect a strong expression or co-expression of CD206 with Dectin-1 in tumor tissues (Fig. 7A and B). Taken together, these findings indicate the abundance of Dectin-1 expressing myeloid cells in tumor tissues.

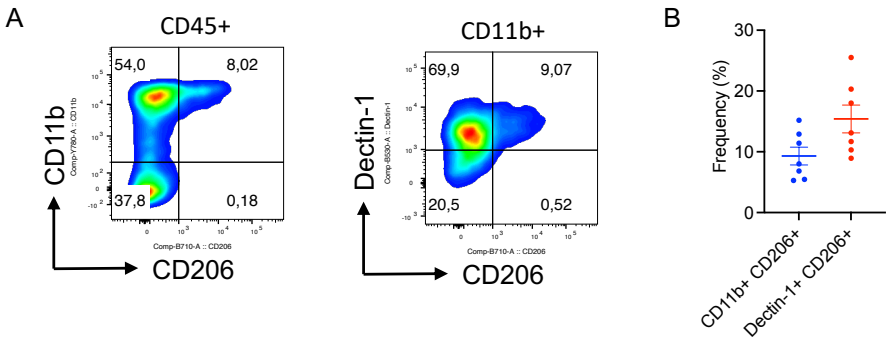

Fig 7. Dectin-1^{+} myeloid cells barely express CD206. (**A**) Representative flow cytometry plots and cumulative data for the expression of CD206 in CD11b^{+} myeloid cells, and co-expression of Dectin-1 with CD206 on CD11b^{+} myeloid cells in the TME. (B) Cumulative data showing frequency of CD11b^{+} CD206^{+} and Dectin-1^{+} CD206^{+} myeloid cells in TME.

Dectin-1$^+$ myeloid cells are highly active and functional in the TME

I aimed to characterize the immune profile of Dectin-1$^+$ myeloid cells compare to their Dectin-1$^-$ counterparts in the TME/spleen by measuring the expression levels of activation markers. Hence, I dichotomized total myeloid cells into Dectin-1$^-$ and Dectin-1$^+$ subsets and measured the expression levels of I-A/I-E, CD80 and CD86 among these subsets. Compared to splenic myeloid cells, I observed remarkable co-expression of I-A/I-E, CD80 and CD86 with Dectin-1 on tumoral myeloid cells in both tumor models (Fig. 8A and B). However, this pattern was completely different in the spleen. For example, I observed significantly a lower percentage of I-A/I-E expressing cells, a higher frequency of CD80 expressing cells without any change in the proportion of CD86 expressing cells among Dectin-1$^+$ myeloid cells in the spleen of B16-F10 tumor model (Fig. 8B).However, Dectin-1$^+$ splenic myeloid cells were significantly enriched with CD80 and CD86 expressing cells without any difference in the frequency of I-A/I-E expressing cells among Dectin-1$^{+/-}$ cells in the CT26 model (Fig. 8B). I further compared these activation markers among Dectin-1$^+$ and Dectin-1$^-$ myeloid cells in the immunogenic and non-immunogenic tumor models. I noticed a significant increase only in the frequency of I-A/I-E between Dectin-1$^+$ and Dectin-1$^-$ myeloid cells in the TME of CT26 but the frequency of CD80 and CD86 expressing myeloid cells remained the same in both models. (Fig. 8C). Surprisingly, splenic Dectin-1$^+$ myeloid cells in the CT26 model had significantly higher proportion of I-A/I-E, CD80, and CD86 expressing cells compared to their counterparts in the B16-F10 model (Fig. 8B).

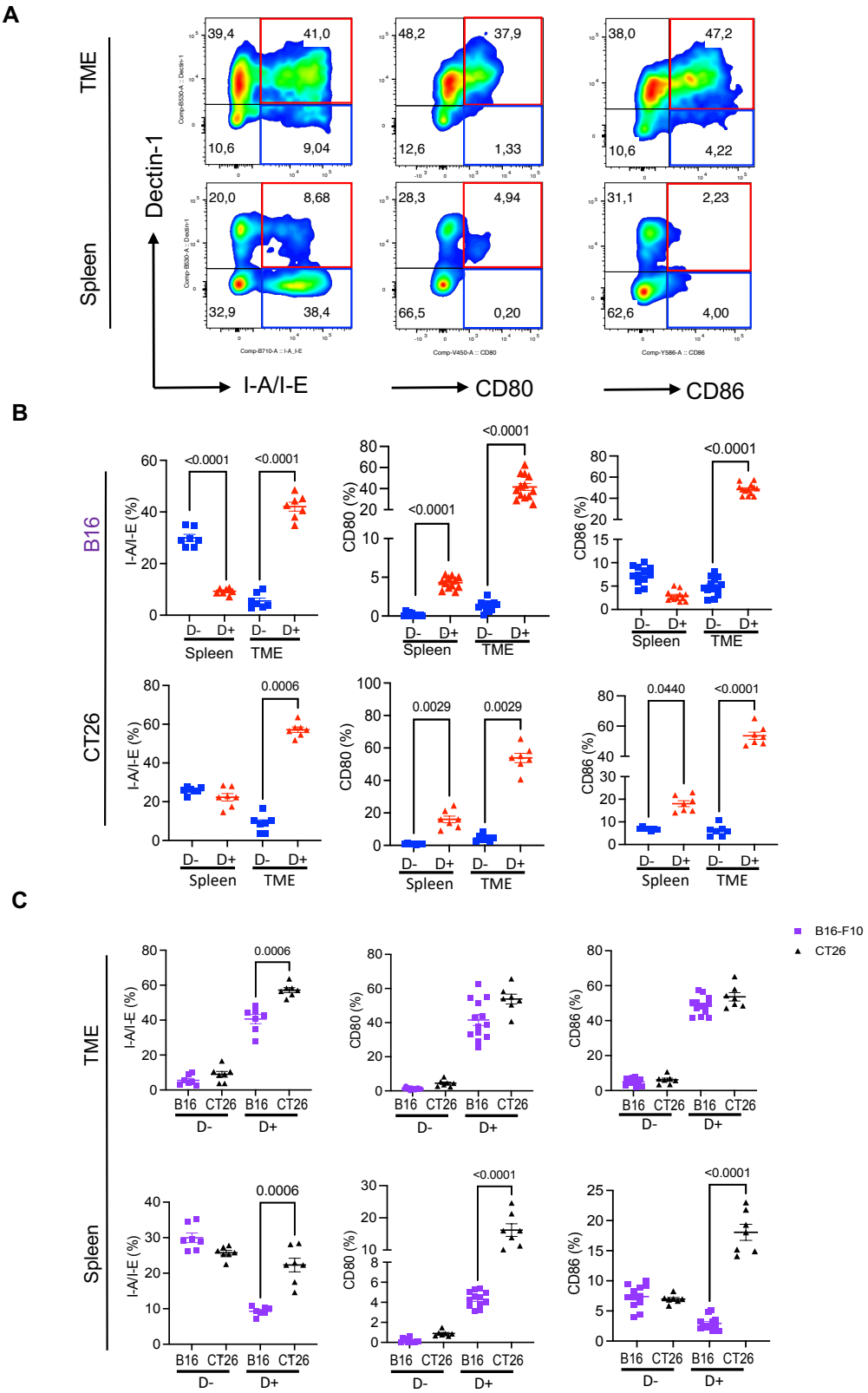
A
TME
Spleen
Dectin-1
I-A/I-E
CD80
CD86
39,4
41,0
10,6
9,04
48,2
37,9
12,6
1,33
38,0
47,2
10,6
4,22
20,0
8,68
32,9
38,4
28,3
4,94
66,5
0,20
31,1
2,23
62,6
4,00
B
B16
CT26
I-A/I-E (%)
CD80 (%)
CD86 (%)
<0.0001
0.0006
0.0029
0.0440
D-
D+
Spleen
TME
C
B16-F10
CT26
B16
CT26
D-
D+

Fig 8. Activated myeloid cells express Dectin-1 but not all Dectin-1$^+$ myeloid cells are active. (**A**) Representative flow cytometry plots for the co-expression of Dectin-1 with I-A/I-E, CD80 and CD86 in CD11b$^+$ myeloid cells in the spleen and TME of B16-F10 tumor-bearing mice. (**B**) Cumulative data of percentages of co-expression of Dectin-1$^+$/Dectin-1$^-$ with I-A/I-E, CD80 and CD86 in CD11b$^+$ myeloid cells in the spleen and TME of B16-F10 and CT26 tumor-bearing mice. (**C**) Cumulative data comparing the percentages of I-A/I-E, CD80 and CD86 expressing cells among Dectin-1$^+$ and Dectin-1$^-$ fractions of myeloid cells in the TME and spleen of CT26 and B16-F10 tumor models.

Moreover, I measured the expression of Arginase-I (Arg-1), ROS, TNF-α, IL-12, IL-10, and Ki67 in freshly isolated immune cells without further stimulation *ex vivo*. In the B16-F10 model, I observed that Dectin-1$^+$ myeloid cells expressed significantly more Arg-I, ROS and TNF-α in the TME, while their counterparts in the spleen expressed significantly higher levels of Arg-I, TNF-α, IL-12 and Ki67 but not ROS (Fig. 9A and B). In the CT26 model, I observed that Dectin-1$^+$ myeloid cells expressed significantly higher levels of Arg-I, TNF-α, IL-12 but lower ROS compared to their Dectin-1- counterparts in the TME (Fig. 9B). However, Dectin-1$^+$ myeloid cells in the spleen had significantly higher expression of Arg-I, IL-12 and Ki67 but lower ROS. At the same time the expression of Ki67 in the TME and TNF-α in the spleen remained unchanged (Fig. 9B). Next, I decided to compare Dectin-1$^+$ and Dectin-1$^-$ myeloid cells in terms of Arg-I, ROS, TNF-α, IL-12, and Ki67 expression in B16-F10 versus CT26. These analyses revealed that myeloid cells regardless of Dectin-1 expression overall had elevated levels of ROS, TNF-α, and Ki67 but lower IL-12 in both tissues (spleen and TME) in B16-F10 versus CT26(Fig. 9C). Taken together, these results suggest that Dectin-1$^+$ myeloid cells appear to exhibit an activated phenotype in the TME but they mainly appear to have immunosuppressive properties in the B16-F10 tumor model, while in CT26 tumor model, they exhibit a pro-inflammatory phenotype. Therefore, Dectin-1 expressing myeloid cells might possess different biological properties in immunogenic and non-immunogenic tumor models.

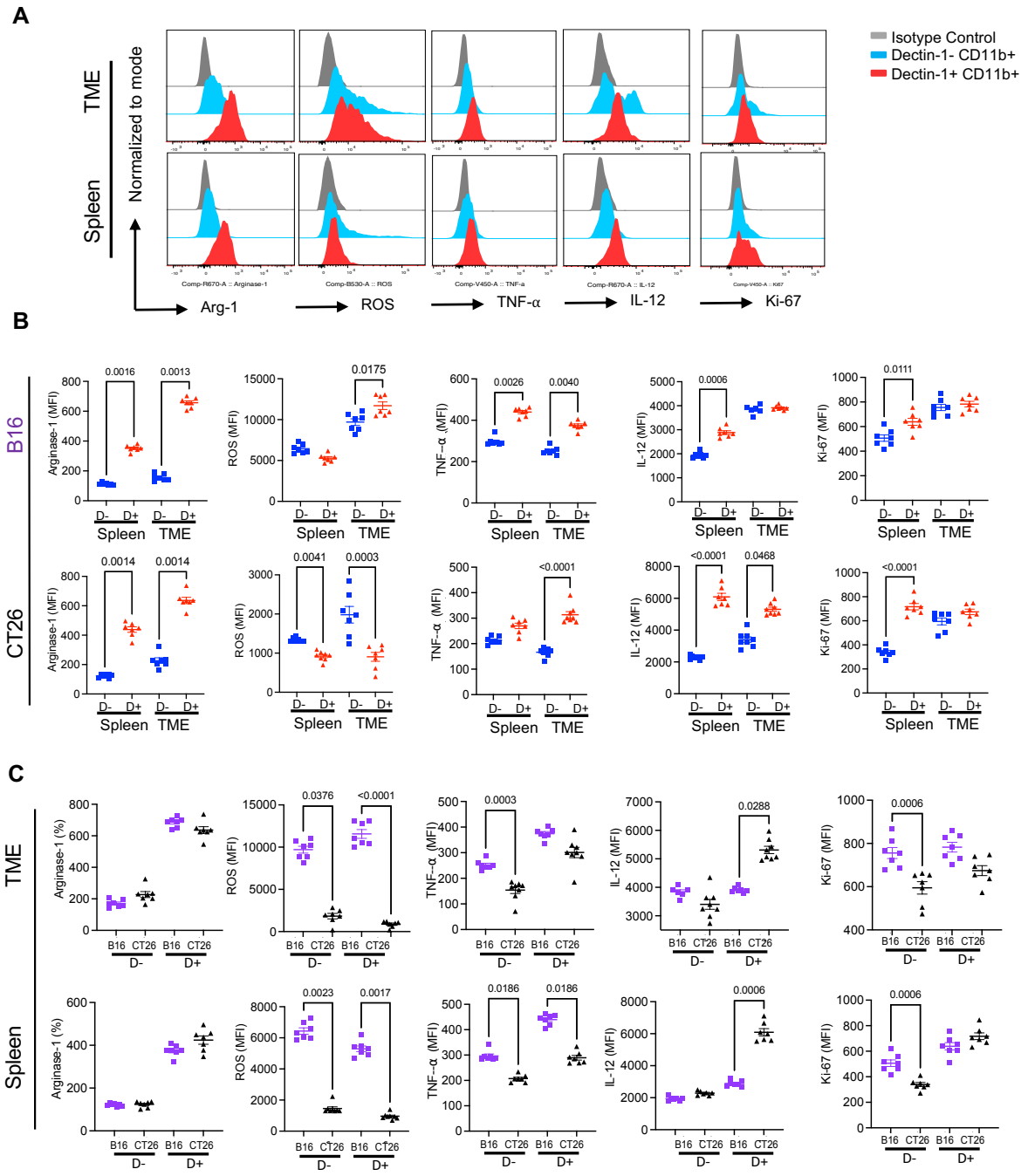

Fig 9. Dectin-1+ myeloid cells express strong amount of ROS, Arg-I and TNF-α in TME. (**A**) Representative histogram plots of Arginase-1 (Arg-1), Reactive Oxygen Species (ROS), TNF-α, IL-12 and Ki-67 expression among Dectin-1^{+}CD11b^{+} and Dectin-1-CD11b^{+} fractions of myeloid cells in the spleen and TME of B16-F10 tumor model. (**B**) Cumulative data showing mean fluorescence intensity (MFI) of Arg-1, ROS, TNF-α, IL-12 and Ki-67 among tumoral and splenic Dectin-1^{+}CD11b^{+} and Dectin-1^{-}CD11b^{+} subsets in B16-F10 and CT26 tumor models. **(C)**Cumulative data of the MFI for Arg-I, ROS, TNF-α, IL-12, and Ki-67 in Dectin-1^{+} and Dectin-1^{-} myeloid cells in B16-F10 vs. CT26 tumor models.

Dectin-1$^+$ myeloid cells express substantial levels of different co-inhibitory receptors in the TME

To further characterize immunological properties of Dectin-1$^+$ myeloid cells in the TME, I subjected them to extensive analysis for the expression of different co-inhibitory molecules. I found that Dectin-1 was significantly co-expressed with PDL-1, PDL-2, VISTA, TIM-3 and Gal-9 in myeloid cells in the TME of both tumor models (Fig. 10A and B). However, this was not the case for Dectin-1 expressing myeloid cells in the spleen. In B16-F10 model, I observed significant upregulation of VISTA and Gal-9 but in CT26, VISTA and TIM-3 were significantly elevated on Dectin-1$^+$ myeloid cells (Fig. 10B). Comparing the immunogenic and non-immunogenic tumor models, I found that Dectin-1$^+$ myeloid cells were significantly enriched with VISTA, TIM-3 and Gal-9 expressing cells in the B16-F10 model while the same subset was significantly enriched with PDL-1 expressing cells in the CT26 model (Fig. 10C). Next, I examined Dectin-1$^+$ myeloid cells in terms of the expression of metabolic associated molecules such as CD39, CD26 and CD73 endonucleases in the TME (Fig. 10D and E). Although tumoral Dectin-1$^+$ myeloid cells expressed elevated levels of CD39 and CD26 and CD73, their siblings in the spleen exhibited unchanged CD39, lower CD26, and higher CD73 expression (Fig. 10C). The strong co-expression of Dectin-1 with PDL-1 and VISTA prompted us to evaluate possible co-localization of these molecules on myeloid subsets. These studies supported substantial co-localization of Dectin-1 with both VISTA and PDL-1 on fresh myeloid cells from the TME (Fig 11A and B). Taken together, my results imply a cross-talk between Dectin-1 and different co-inhibitory receptors/ligands, which may influence myeloid cell effector functions in the TME.

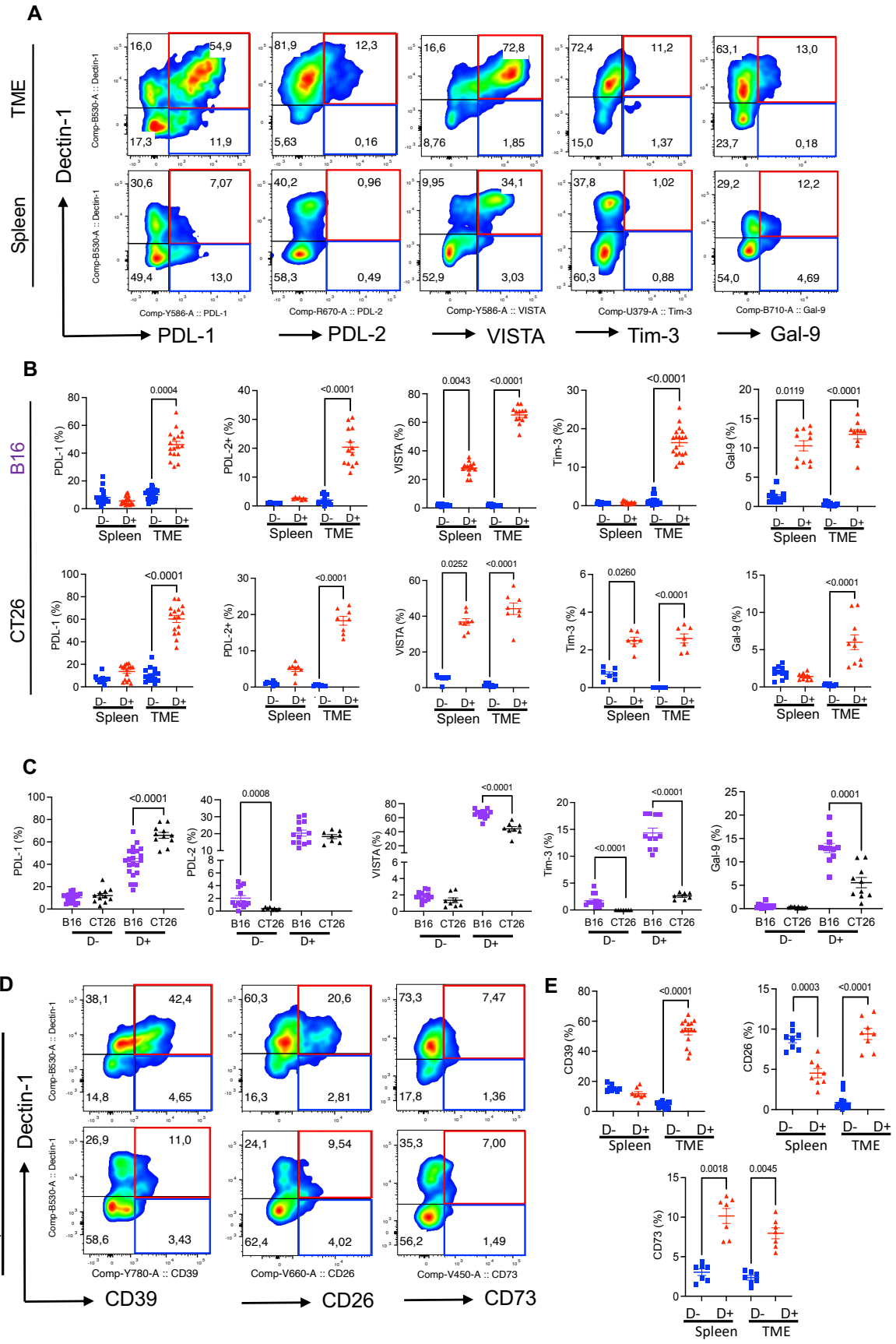
A
TME
Spleen
Dectin-1
PDL-1
PDL-2
VISTA
Tim-3
Gal-9
B
B16
CT26
PDL-1 (%)
PDL-2+ (%)
VISTA (%)
Tim-3 (%)
Gal-9 (%)
Spleen
TME
C
B16
CT26
D-
D+
D
CD39
CD26
CD73
E
CD39 (%)
CD26 (%)
CD73 (%)

Fig 10. Dectin-1$^+$ myeloid cells strongly express co-inhibitory receptors in TME but not spleen. (**A**) Representative flow cytometry plots for tumoral and splenic co-expression of Dectin-1 with PDL-1, PDL-2, VISTA, TIM-3 and Gal-9 among CD11b$^+$ myeloid cells in the TME and spleen of B16-F10 tumor model. (**B**) Cumulative data showing the percentages of PDL-1, PDL-2, VISTA, TIM-3 and Gal-9 expressing cells among Dectin-1$^+$CD11b$^+$ and Dectin-1-CD11b$^+$ subsets in the spleen and TME of B16-F10 tumor model. (**C**) Cumulative data comparing percentages of PDL-1, PDL-2, VISTA, Tim-3 and Gal-9 expressing cells among Dectin-1$^+$ and Dectin-1$^-$ myeloid subsets in B16-F10 and CT26 tumor models. (**D**) Representative flow cytometry plots for co-expression of Dectin-1 with CD39, CD26 and CD73 in myeloid cells in the TME and Spleen of the B16-F10 tumor model. (**E**) Cumulative data of percentages of CD39, CD26 and CD73 expressing cells among Dectin-1$^+$ and Dectin-1$^-$ myeloid subsets in the spleen and TME of the B16-F10 tumor model.

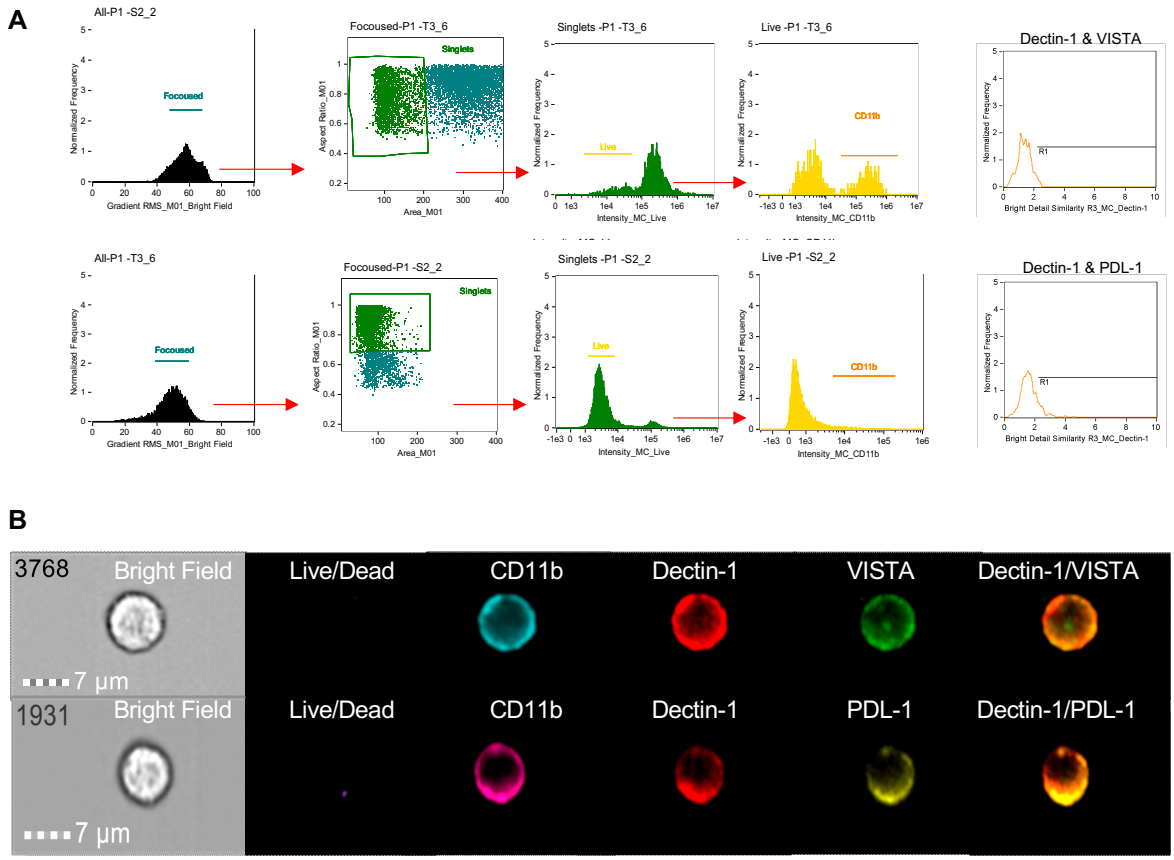

Fig 11. Dectin-1$^+$ is co-localized with PDL-1 and VISTA on myeloid cells. (**A**) Representative Image cytometry plots showing the gating strategy for calculating co-localization of Dectin-1 and PDL-1/VISTA in myeloid cells in the TME. (**B**) Image stream plots of surface co-localization of Dectin-1 and VISTA or Dectin-1 and PDL-1 on the surface of CD11b$^+$ myeloid cells from the TME of B16-F10 tumor model.

Dectin-1$^+$ myeloid cells are localized in the margin of the tumor tissue

The pattern of TILs is an important factor associated with the cancer progression (81)(82). Likewise, immune disposition in the tumor centre or periphery, and the density and pattern of TILs are associated with the tumor outcomes (83)(84). Therefore, I performed IF staining to determine the localization of Dectin-1$^+$ myeloid cells (CD11b$^+$) versus Dectin-1- myeloid cells. I observed that although CD11b$^+$ cells were distributed in the periphery and the tumor centre, Dectin-1$^+$CD11b$^+$ cells were mainly deposited in the periphery (Fig. 12A). These observations indicate that Dectin-1$^+$CD11b$^+$ cells are located at the invasive tumor front (Fig. 12B). rather than the tumor centre in the B16-F10 model.

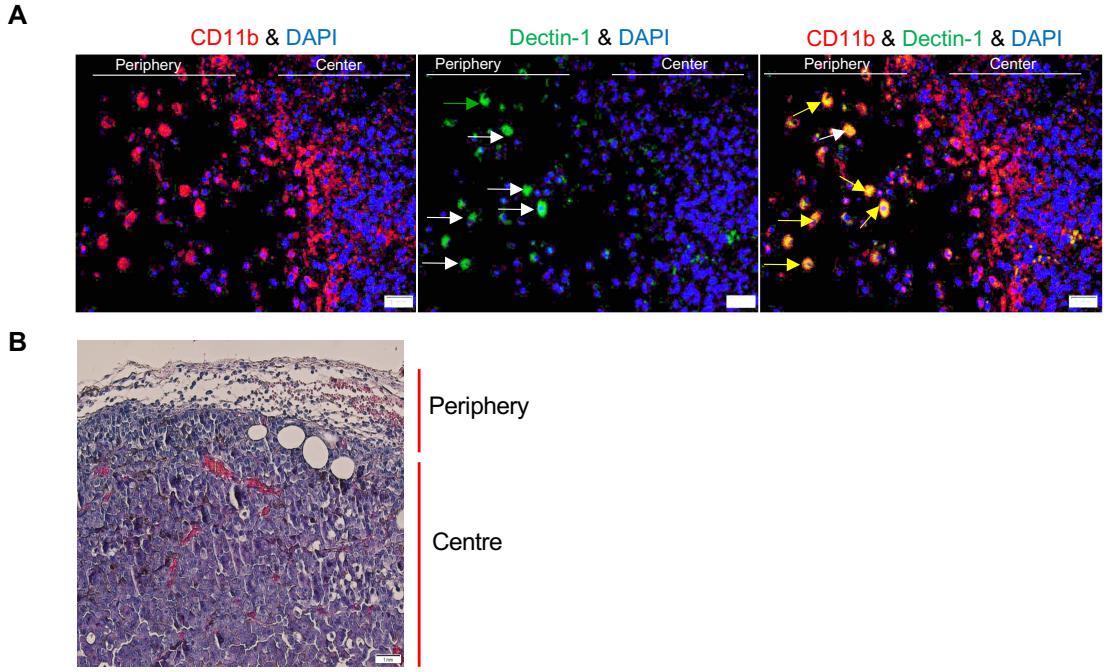

Fig 12. Dectin-1$^+$ myeloid cells are distributed in the periphery. **(A)** Representative images of the immunofluorescent staining (IF) for CD11b, Dectin-1 and DAPI in B16-F10 tumor tissue. **(B)** Representative images of the H&E staining of B16-F10 tumor tissue.

Dectin-1$^+$ effector T cells are present in the TME and express co-inhibitory receptors

It is reported that CCR6$^+$IL-17-producing gamma-delta T cells express TLR-2 and Dectin-1(85). Based on this report, I decided to analyze the presence of Dectin-1$^+$ T cells in B16-F10 model because of a greater frequency of these cells in this model. My studies revealed the presence of a subset of CD3$^+$ and subsequently CD4$^+$ and CD8$^+$ T cells expressing Dectin-1 in the TME, however, Dectin-1$^+$ T cells were very scarce in the spleen (Fig. 13A and 13B). Although a subset of both CD4$^+$ and CD8$^+$ T cells in the TME expressed Dectin-1, CD4$^+$ T cells were the dominant T cell subset having significantly higher frequency of Dectin-1$^+$ cells in the TME of both B16-F10 and CT26 models (Fig. 13A and 13B). However, the intensity of Dectin-1 was almost at the same level on CD3$^+$, CD4$^+$ and CD8$^+$ T cells (Fig. 13C and 13D). Moreover, I compared the frequency of Dectin-1$^+$ T cells in the TME and spleen of B16-F10 versus CT26 tumor model. I found that Dectin-1$^+$ CD3$^+$, CD4$^+$ and CD8$^+$ were significantly enriched in the TME and spleen of B16-F10 mice compared to CT26 (Fig. 13E). My further analysis revealed that Dectin-1$^+$ T cells had a heterogeneous phenotype exhibited by the expression of different T cells-associated transcriptional factors such as GATA3, T-bet and RORγt (Fig 13F and 13G). These observations suggest that Dectin-1$^+$ CD3$^+$ T cells do not possess a unique transcriptional signature. Moreover, to better understand effector functions of Dectin-1$^+$ CD3$^+$ T cells, I subjected them to immune phenotyping and found that Dectin-1$^+$ T cells had mainly an effector phenotype compared to Dectin-1- CD3$^+$ T cells in the TME (Fig. 14A and 14B). However, Dectin-1$^+$ CD3$^+$ T cells had a combination of memory and effector phenotype in the spleen (Fig. 14A and 14B). Because of the effector phenotype of Dectin-1$^+$ CD3$^+$ T cells in the TME, I decided to subject them to further analysis for the expression co-inhibitory receptors. I found that Dectin-1$^+$ CD3$^+$ T cells expressed significantly higher levels of CTLA-4, LAG-3, TIM-3, VISTA, and Gal-9 compared to their negative counterparts in the TME (Fig. 15A and 15B). Not only the intensity of co-inhibitory receptors expression but also the proportion of T cells expressing co-inhibitory receptors was significantly higher in Dectin-1$^+$ T cells compared to their Dectin-1- counterparts (Fig. 15E and 15F). I observed almost the same pattern for the expression of these co-inhibitory receptors on CD4$^+$ and CD8$^+$ T cells in the TME as they exhibited significantly higher intensity of CTLA-4, LAG-3, TIM-3, VISTA and Gal-9 compared to Dectin-1- CD4$^+$ and CD8$^+$ T cells in the TME (Fig. 15C and 15D). Collectively these results imply that Dectin-1$^+$ T cells express elevated levels of co-inhibitory receptors compared to their Dectin-1$^-$ siblings.

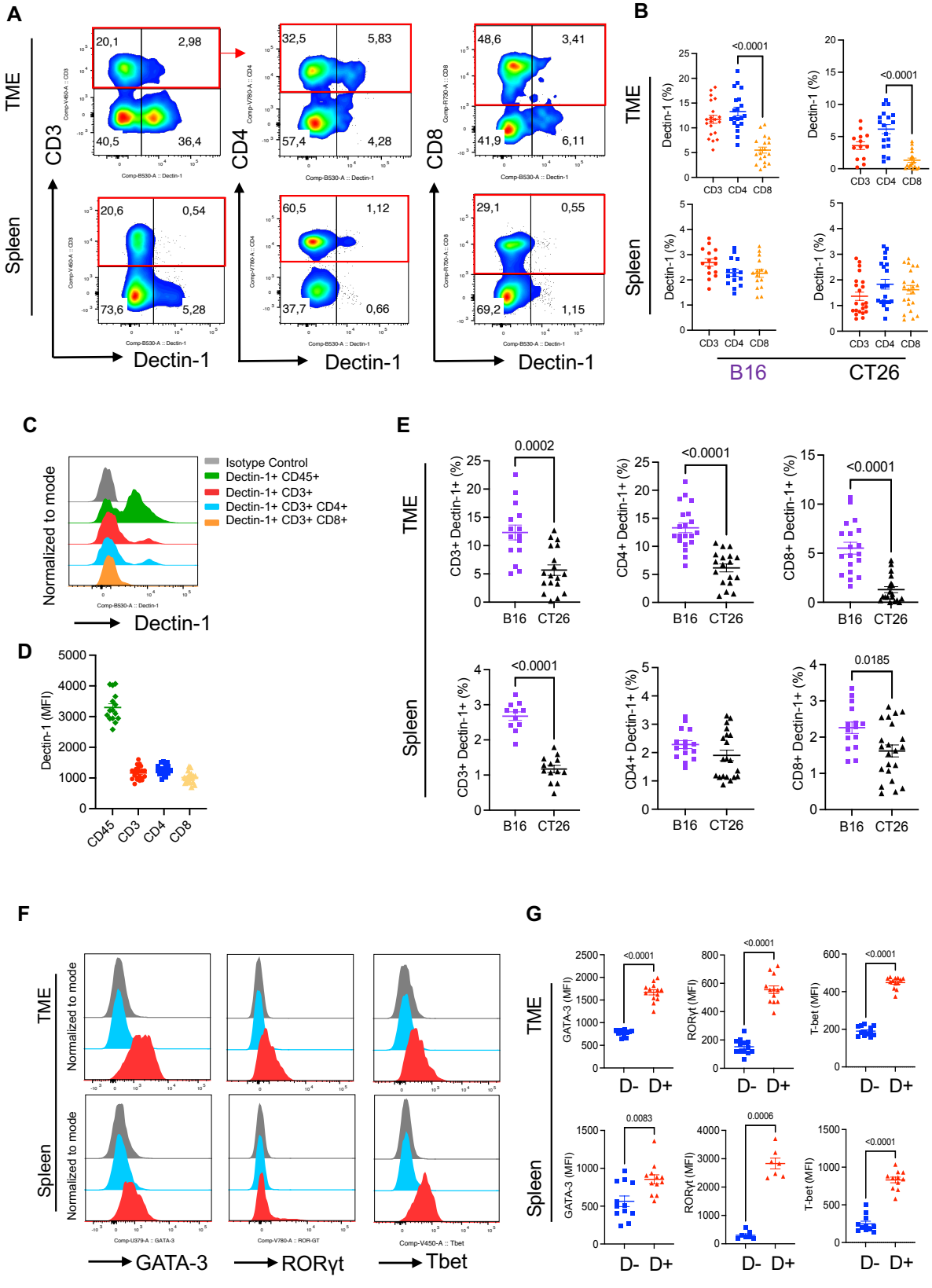
A
TME
Spleen
CD3
CD4
CD8
20,1
2,98
40,5
36,4
32,5
5,83
57,4
4,28
48,6
3,41
41,9
6,11
20,6
0,54
73,6
5,28
60,5
1,12
37,7
0,66
29,1
0,55
69,2
1,15
Dectin-1
B
Dectin-1 (%)
<0.0001
CD3 CD4 CD8
B16
CT26
C
Normalized to mode
Isotype Control
Dectin-1+ CD45+
Dectin-1+ CD3+
Dectin-1+ CD3+ CD4+
Dectin-1+ CD3+ CD8+
Dectin-1
D
Dectin-1 (MFI)
CD45 CD3 CD4 CD8
E
CD3+ Dectin-1+ (%)
CD4+ Dectin-1+ (%)
CD8+ Dectin-1+ (%)
0.0002
<0.0001
0.0185
B16 CT26
F
Normalized to mode
GATA-3
RORγt
Tbet
G
GATA-3 (MFI)
RORγt (MFI)
T-bet (MFI)
0.0083
0.0006
D- D+

Fig 13. Dectin-1 mainly expressed on CD4 T cells in TME. (**A**) Representative flow cytometry plots of Dectin-1 expressing cells among $CD3^+$, $CD4^+$ and $CD8^+$ T cells in the TME of B16-F10 tumor model. (**B**) Cumulative data of percentages of Dectin-1^+ cells among $CD3^+$, $CD4^+$ and $CD8^+$ T cells in the TME and spleen of B16-F10 and CT26 tumor models. (**C**) Representative histogram plots, and (**D**) cumulative data of MFI for Dectin-1 expression among $CD45^+$ immune cells versus $CD3^+$, $CD4^+$ and $CD8^+$ T cells in the TME of B16-F10 tumor model. (**E**) Cumulative data comparing percentages of Dectin-1 expressing T cells in B16-F10 and CT26 tumor models. **(F)** Representative histogram plots of GATA-3, RORγt and Tbet in Dectin-1^- and Dectin-1^+ subsets of T cells in in the TME and Spleen. (**G**) Cumulative data of the MFI of GATA-3, RORγt and Tbet in Dectin-1^- and Dectin-1^+ subsets of T cells in the TME and spleen.

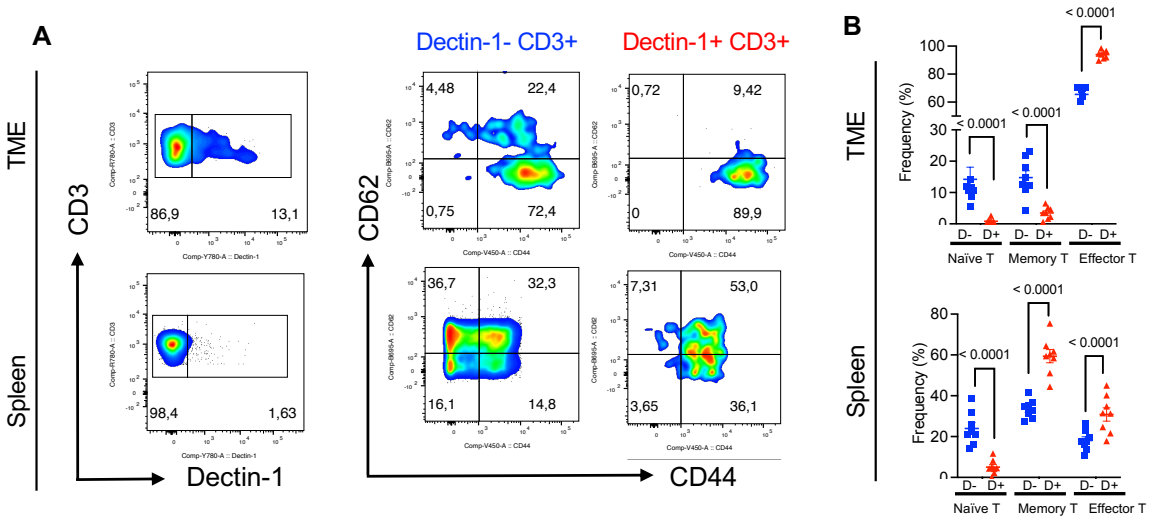

Fig 14. Dectin-1^+ T cells show effector phenotype (**A**) Representative flow cytometry plots, and (**B**) cumulative data of percentages of Dectin-1^+ naïve, memory and effector T cells in the TME and spleen of B16-F10 tumor model.

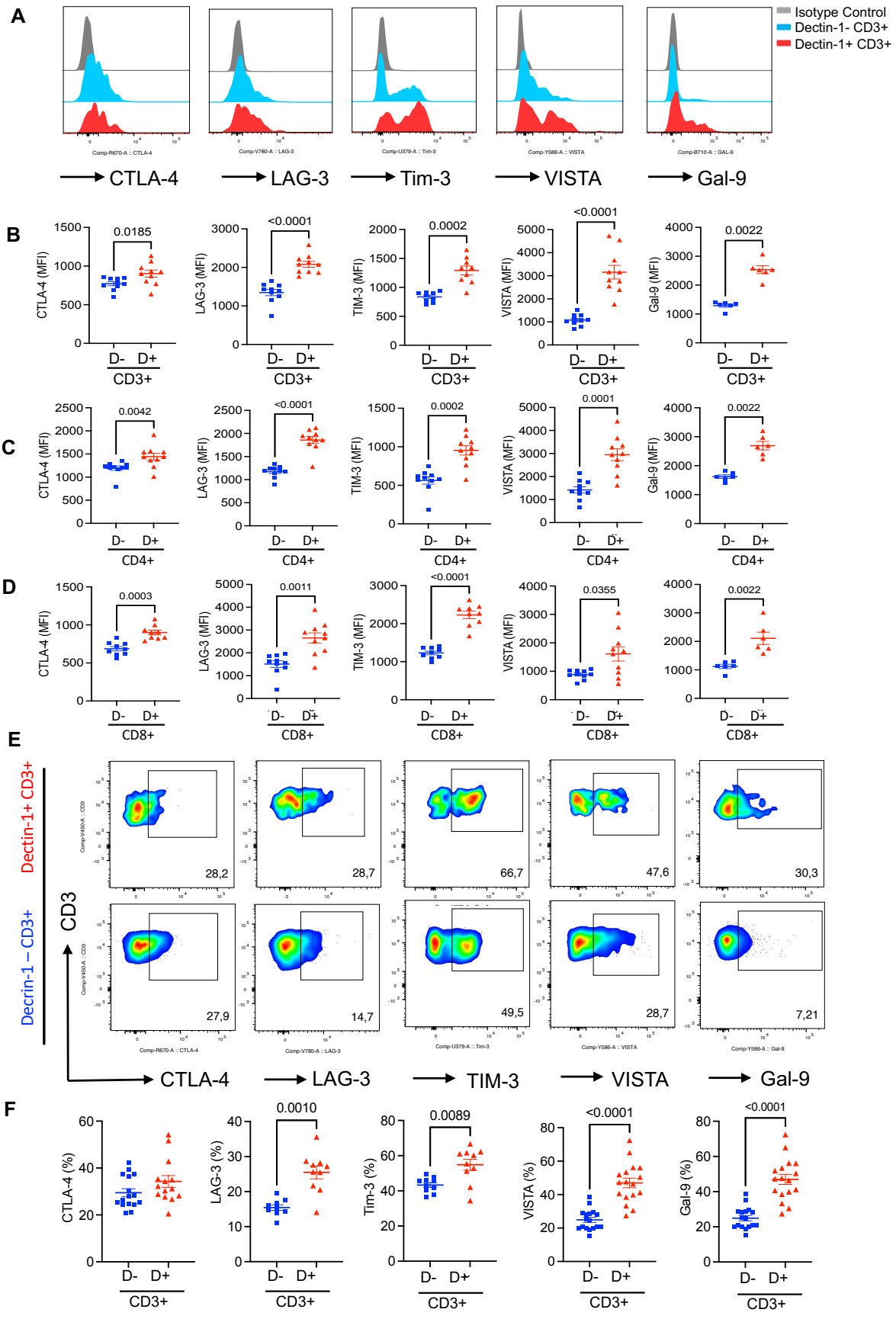
A
Isotype Control
Dectin-1- CD3+
Dectin-1+ CD3+
CTLA-4
LAG-3
Tim-3
VISTA
Gal-9
B
CTLA-4 (MFI)
LAG-3 (MFI)
TIM-3 (MFI)
VISTA (MFI)
Gal-9 (MFI)
0.0185
<0.0001
0.0002
<0.0001
0.0022
D- D+
CD3+
C
0.0042
<0.0001
0.0002
0.0001
0.0022
CD4+
D
0.0003
0.0011
<0.0001
0.0355
0.0022
CD8+
E
Dectin-1+ CD3+
Decrin-1 – CD3+
CD3
28,2
28,7
66,7
47,6
30,3
27,9
14,7
49,5
28,7
7,21
CTLA-4
LAG-3
TIM-3
VISTA
Gal-9
F
CTLA-4 (%)
LAG-3 (%)
Tim-3 (%)
VISTA (%)
Gal-9 (%)
0.0010
0.0089
<0.0001
<0.0001
D- D+
CD3+

Fig 15. Dectin-1$^+$ effector T cells are present in the TME and express co-inhibitory receptors. (**A**) Representative histogram plots, and (**B**) cumulative data of the MFI for CTLA-4, LAG-3, TIM-3, VISTA and Gal-9 in Dectin-1$^+$CD3$^+$ T cells versus Dectin-1-CD3$^+$ T cells in the TME of B16-F10 tumor model. (**C**) Cumulative data of the MFI for CTLA-4, LAG-3, Tim-3, VISTA and Gal-9 on Dectin-1$^+$ CD4$^+$ and Dectin-1$^-$ CD4$^+$ T cells in the TME. (**D**) Cumulative data of the MFI for CTLA-4, LAG-3, Tim-3, VISTA and Gal-9 on Dectin-1$^+$ CD8$^+$ and Dectin-1$^-$ CD8$^+$ T cells in the TME. (**E**) Representative flow cytometry plots showing surface expression of CTLA-4, LAG-3, Tim-3, VISTA and Gal-9 on Dectin-1$^+$ CD3$^+$ and Dectin-1$^-$ CD3$^+$ T cells in the TME. (**F**) Cumulative data of percentages of CTLA-4, LAG-3, TIM-3, VISTA and Gal-9 expressing T cells among Dectin-1$^+$CD3$^+$ T cells and Dectin-1-CD3$^+$ T cells in the TME of B16-F10 tumor model.

The combination of curdlan and/or the anti-VISTA antibody enhances overall immune responses in the B16-F10 model

Given the controversial role of Dectin-1 in cancer progression (54)(67), I decided to target Dectin-1 by curdlan , its commonly used agonist, *in vivo*. For this purpose, B16-F10 tumor bearing wild type (WT) mice were treated (i.p.) with curdlan (15 mg/kg) starting one day after tumor inoculation every 3 days for a total of five treatments as illustrated in Fig. 16A. Also, I used DKO mice as another control group to compare the absence versus antagozing of Dectin-1 in B16-F10 model. I observed that the tumor volume was not significantly different in WT versus DKO mice, however, treatment with curdlan significantly reduced the tumor size and tumor weight in WT mice (Fig. 16B-D). In parallel, I found that curdlan-treated mice showed significantly enlarged spleen size, while no significant difference was noted between WT and DKO mice (Fig. 16E and 16F). Immunological assessment of splenocytes and immune cells from the TME indicated that curdlan treatment significantly increased the proportion of CD4$^+$ and CD8$^+$ T cells in the TME, however, it did not impact the proportion of CD11b$^+$ (Fig. 16G). Also, I found that curdlan treatment significantly increased the proportion of CD4$^+$ T cells and CD11b$^+$ cells but in contrast reduced the frequency of CD8$^+$ T cells in the spleen of mice (Fig. 16G). Although the frequency of CD11b$^+$ cells remained unchanged, this treatment was associated with increased TNF-α, IFN-γ and IL-12 expression by total CD11b$^+$ cells in the TME and spleen of WT mice (Fig. 16H). It is worth mentioning that CD11b$^+$ cells in DKO mice exhibited significantly lower expression of TNF-α, IFN-γ and IL-12 cytokines in their spleens and TMEs (Fig. 16H). I also noticed that curdlan treatment significantly reduced the percentages of VISTA$^+$ and PDL-1$^+$ CD11b cells in the TME but only VISTA$^+$ CD11b$^+$ cells in the spleen (Fig. 16I). I further analyzed the effects of curdlan

treatment on T cell functions in tumor-bearing mice. I observed that expanded $CD4^+$ T cells in curdlan treated mice expressed significantly higher levels of only TNF-α but no other cytokines (Fig. 16J). However, this treatment had no significant effects on the expression of cytotoxic molecules (e.g. granzym B and perforin) in $CD8^+$ T cells in the TME and spleen (Fig. 16K). Because of a substantial co-expression of VISTA with Dectin-1 on $CD11b^+$ cells (Fig. 10A and 10B) and substantial reduction in its expression following curdlan treatment (Fig. 16I), I decided to better delineate the role of VISTA in this model.

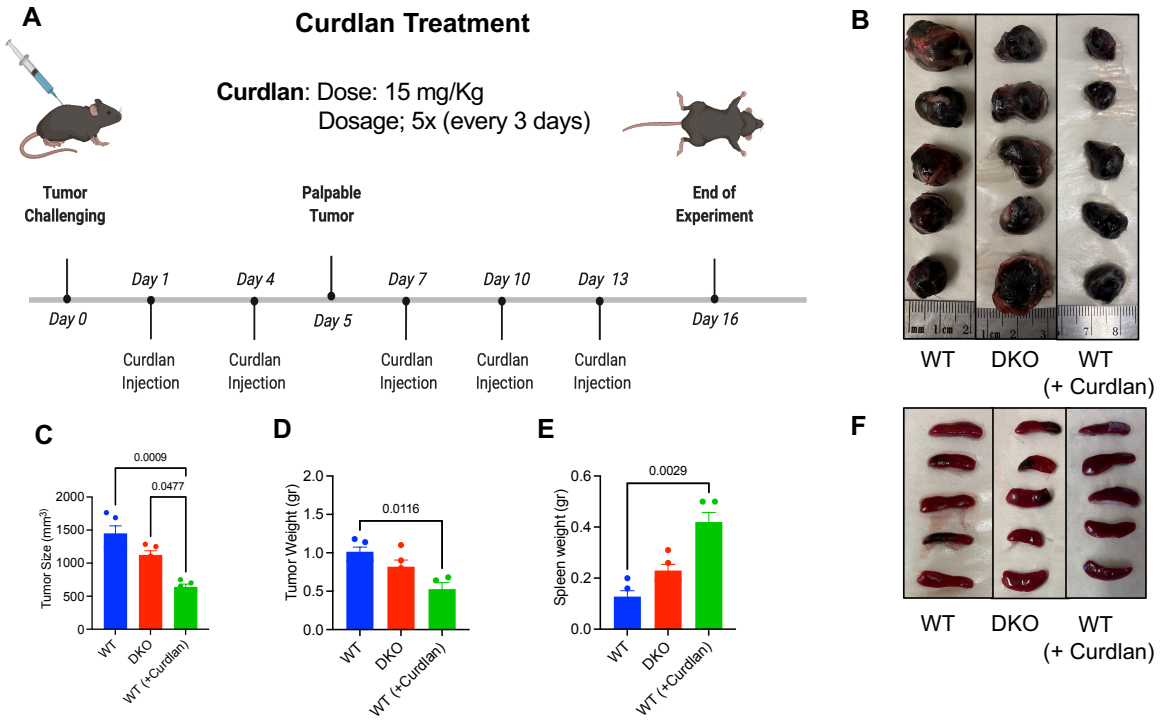
A
Curdlan Treatment
Curdlan: Dose: 15 mg/Kg
Dosage; 5x (every 3 days)
Tumor Challenging
Palpable Tumor
End of Experiment
Day 0
Day 1
Day 4
Day 5
Day 7
Day 10
Day 13
Day 16
Curdlan Injection
B
WT
DKO
WT (+ Curdlan)
C
Tumor Size (mm³)
D
Tumor Weight (gr)
E
Spleen weight (gr)
F
G
TME
Spleen
CD4 (%)
CD8 (%)
CD11b (%)
H
TNF-α (MFI)
IFN-γ (MFI)
IL-12 (MFI)
I
VISTA (%)
PDL-1 (%)
J
K
GrzB (MFI)
Perforin (MFI)

Fig 16. Targeting Dectin-1 by curdlan enhances overall immune responses in the B16-F10 tumor model. (**A**) Schematic picture of treatment schedule for WT tumor-bearing mice. (**B**) Representative pictures of dissected tumor tissues from WT tumor-bearing mice, DKO tumor-bearing mice, and curdlan-treated tumor-bearing mice. (**C**) Cumulative data showing tumor size in wild type (WT) tumor-bearing mice, Dectin-1 KO (DKO) tumor-bearing mice, and curdlan-treated tumor-bearing mice. (**D**) Cumulative data showing tumor weight in WT tumor-bearing mice, DKO tumor-bearing mice, and curdlan-treated tumor-bearing mice. (**E**) Cumulative data showing the spleen weight in WT tumor-bearing mice, DKO tumor-bearing mice, and curdlan-treated tumor-bearing mice. (**F**) Representative images of spleens of WT, DKO and curdlan-treated WT tumor-bearing mice. (**G**) Cumulative data comparing the frequency of $CD4^+$ T cells, $CD8^+$ T cells and $CD11b^+$ myeloid cells among WT, DKO and curdlan-treated WT tumor-bearing mice in the TME and spleen. (**H**) Cumulative data of the MFI for TNF-α, IFN-γ and IL-12 expression among $CD11b^+$ myeloid cells from the TME and spleen of WT tumor-bearing mice, DKO tumor-bearing mice, and curdlan-treated tumor-bearing mice. (**I**) Cumulative data of percentages of VISTA and PDL-1 expressing cells among $CD11b^+$ myeloid cells from the TME and spleen of WT tumor-bearing mice, DKO tumor-bearing mice, and WT curdlan-treated tumor-bearing mice. (**J**) Cumulative data of the MFI of TNF-α expression in $CD4^+$ T cells among WT, DKO and curdlan-treated WT tumor-bearing mice in the TME and spleen. (**K**) Cumulative data of the MFI of GrzB and Perforin expression in $CD8^+$ T cells among WT, DKO and curdlan-treated WT tumor-bearing mice in the TME and spleen.

It is well-documented that blocking VISTA can result in a robust immune response against cancer (86)(87). Therefore, I decided to perform a comprehensive study by investigating the role of curdlan in WT and VISTA KO mice. For this purpose, I first compared tumor size in WT, WT treated with curdlan (15mg/kg), VISTA KO mice, WT treated with curdlan (15mg/kg) plus anti-VISTA antibody (250 μg/mouse) (Fig. 17A). As anticipated, the tumor size/weight was significantly smaller in VISTA KO mice compared to their WT counterparts (Fig. 17B, 17C and 17D). However, the combination therapy with the anti-VISTA neutralizing antibody plus curdlan did not induce any synergistic effects on reducing the tumor mass (Fig. 17B, 16C and 17D). I noted that a reduction in tumor volume was associated with an increase in the spleen size (Fig. 17E and 17F). Analysis of immune cell proportions in the TME revealed significantly higher percentages of $CD4^+$ and $CD8^+$ T cells in the TME of VISTA KO and WT mice treated with curdlan (Fig. 17G). At the same time, I noted an increase in the NK cell population in the TME of only VISTA KO and WT treated with curdlan plus anti-VISTA antibody (Fig. 17G). However, I found an increase in $CD4^+$ T cell percentages in WT treated mice once treated with curdlan without any significant increase in $CD8^+$ T cells in the spleen (Fig. 17G). Also, I observed an increase in NK

cell proportion in the TME of VISTA KO and WT mice treated with the anti-VISTA antibody plus curdlan compared to the WT group (Fig. 17G). Although $CD11b^+$ cells remained unchanged in the TME, I found a significant expansion of these cells in the spleen of WT mice treated with curdlan and those treated with curdlan plus anti-VISA antibody compared to the WT group (Fig 17G). In terms of cytokine expression, I did not see a clear picture when different groups were compared to each other. Unlike curdlan-treated mice that showed enhanced IFN-γ and IL-12 expression in their $CD11b^+$ in the TME and spleen, VISTA KO and double treated mice exhibited higher IFN-γ in $CD11b^+$ in their spleens only (Fig. 18A). In $CD4^+$ T cells, when four groups were compared to each other in terms of cytokine expression I did not observe a clear picture; but I noted a higher expression of TNF-α and IFN-γ in VISKA KO compared to the WT group in the TME (Fig. 18B). It appeared that $CD8^+$ T cells exhibited a greater GzmB and perforin expression only in the VISTA KO group (Fig. 18B).

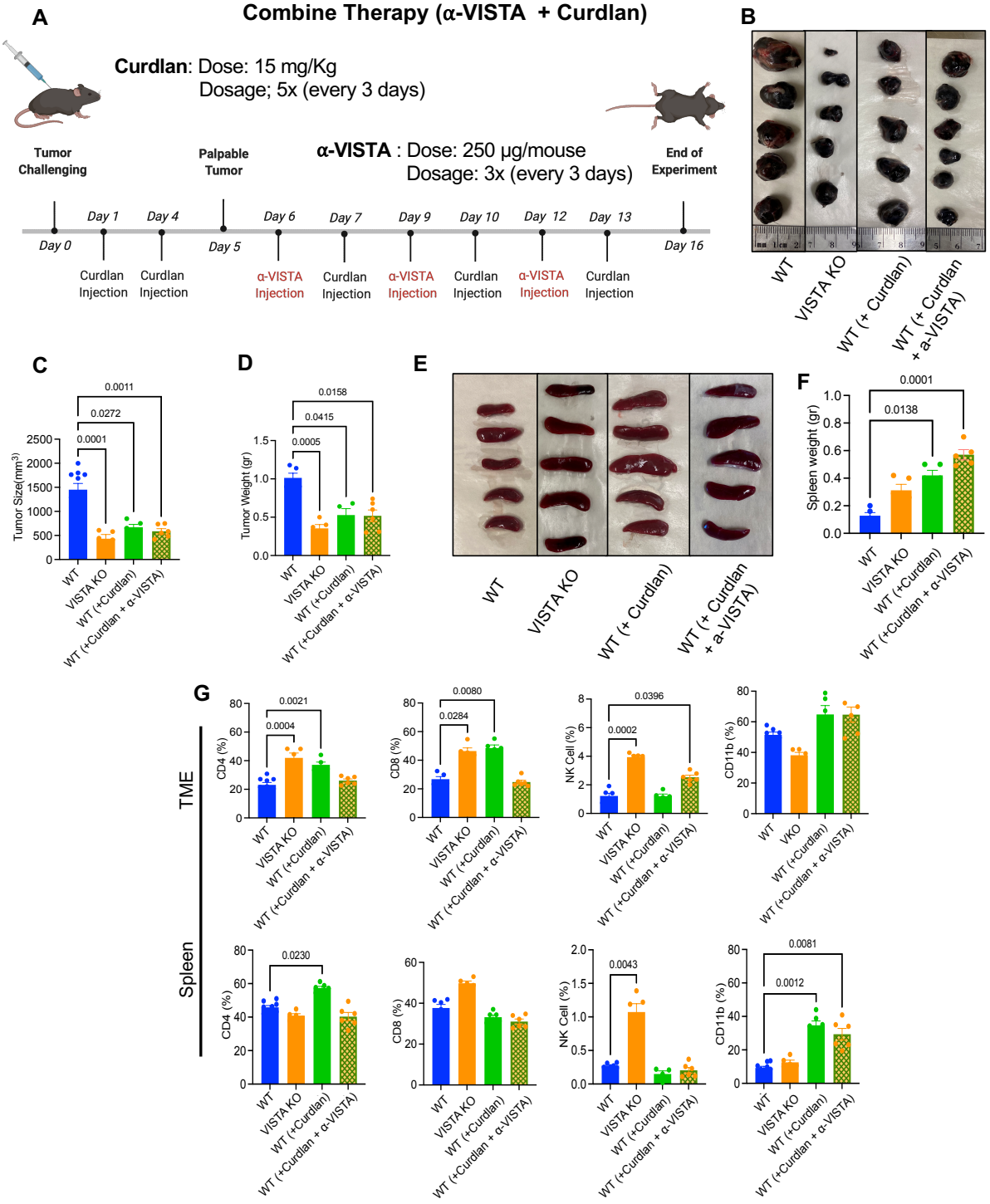
A
Combine Therapy (α-VISTA + Curdlan)
Curdlan: Dose: 15 mg/Kg
Dosage; 5x (every 3 days)
α-VISTA : Dose: 250 μg/mouse
Dosage: 3x (every 3 days)
Tumor Challenging
Palpable Tumor
End of Experiment
Day 0
Day 1
Day 4
Day 5
Day 6
Day 7
Day 9
Day 10
Day 12
Day 13
Day 16
Curdlan Injection
α-VISTA Injection
B
WT
VISTA KO
WT (+ Curdlan)
WT (+ Curdlan + a-VISTA)
C
Tumor Size(mm3)
D
Tumor Weight (gr)
E
F
Spleen weight (gr)
G
TME
Spleen
CD4 (%)
CD8 (%)
NK Cell (%)
CD11b (%)
VKO

Fig 17. Treatment with Curdlan and anti-VISTA combine didn't show synergistic effect in B16-F10 tumor-bearing mice. (**A**) Schematic picture of treatment schedule for WT tumor-bearing mice with curdlan and α-VISTA (anti-VISTA) monoclonal antibody. (**B**) Representative picture of dissected tumor tissue from WT tumor-bearing mice, VISTA KO tumor-bearing mice, WT curdlan-treated tumor-bearing mice and combined (curdlan $^{+}$ anti-VISTA antibody) treated WT tumor-bearing mice. (**C**) Cumulative data showing tumor size in WT tumor-bearing mice, VISTA KO tumor-bearing mice, WT curdlan-treated tumor-bearing mice and combined (curdlan + anti-VISTA antibody) treated WT tumor-bearing mice. (**D**) Cumulative data of tumor weight in WT tumor-bearing mice, VISTA KO tumor-bearing mice, WT curdlan-treated tumor-bearing mice and combined treated WT tumor-bearing mice. (**E**) Representative images of spleens of WT, VISTA KO, curdlan-treated WT and curdlan plus α-VISTA treated WT tumor-bearing mice. (**F**) Cumulative data of spleen weight in WT tumor-bearing mice, VISTA KO tumor-bearing mice, WT curdlan-treated tumor-bearing mice and combined (curdlan + anti-VISTA antibody) treated WT tumor-bearing mice. (**G**) Cumulative data of the frequency of $CD4^{+}$ T cells, $CD8^{+}$ T cells, NK cells and $CD11b^{+}$ myeloid cells among WT, VISTA KO, curdlan-treated WT and curdlan plus α-VISTA treated WT tumor-bearing mice. (**G**) Cumulative data showing tumor size in WT tumor-bearing mice, VISTA KO tumor-bearing mice, WT curdlan-treated tumor-bearing mice and combined (curdlan + anti-VISTA antibody) treated WT tumor-bearing mice. (**H**) Cumulative data of tumor weight in WT tumor-bearing mice, VISTA KO tumor-bearing mice, WT curdlan-treated tumor-bearing mice and combined treated WT tumor-bearing mice.

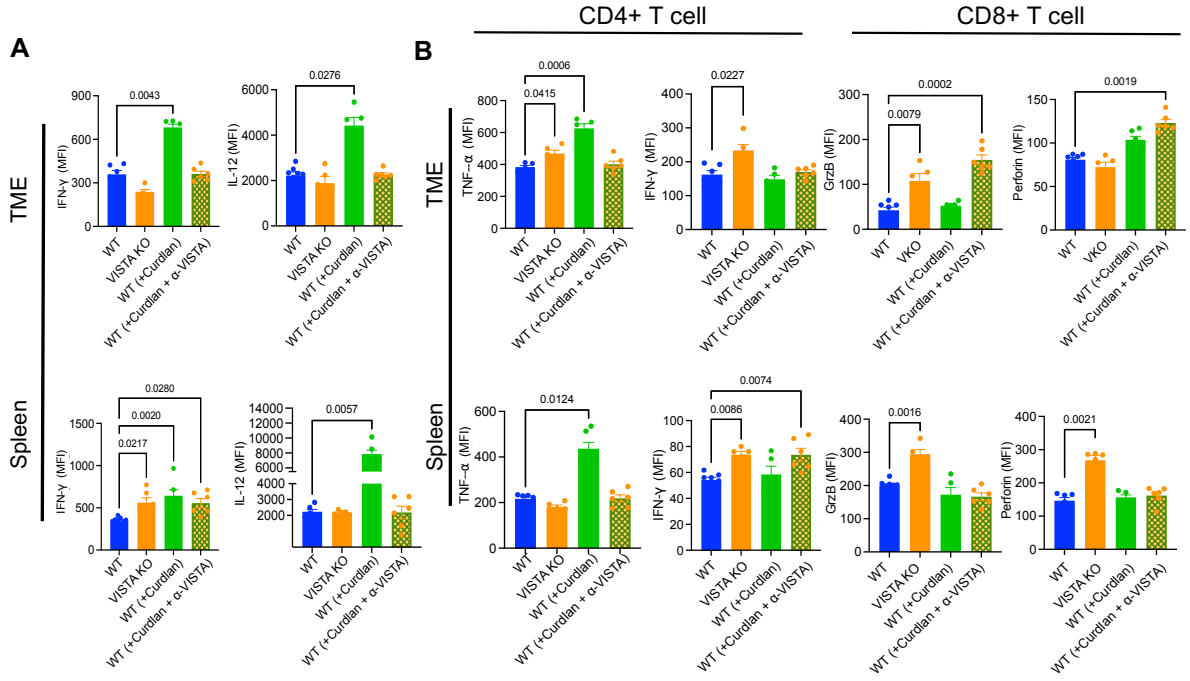

Fig 18. Cytokine expression profile of monotherapies and combination therapy in B16-F10 tumor-bearing mice. (**A**) Cumulative data of the MFI of TNF-α and IL-12 in tumoral and splenic CD11b$^+$ myeloid cells among WT, VISTA KO, curdlan-treated WT and curdlan plus α-VISTA treated WT tumor-bearing mice. (**B**) Cumulative data of the MFI for TNF-α and IFN-γ in tumoral and splenic CD11b$^+$ myeloid cells among WT, VISTA KO, curdlan-treated WT and curdlan plus α-VISTA treated WT tumor-bearing mice and cumulative data comparing the MFI of GrzB and Perforin in tumoral and splenic CD8$^+$ T cells among WT, VISTA KO, curdlan-treated WT and curdlan plus α-VISTA treated WT tumor-bearing mice.

Since VISTA was highly co-expressed with Dectin-1 (Fig. 10A and 10B), I decided to investigate whether neutralizing VISTA can influence the tumor growth in DKO mice. I found that treatment of DKO with the anti-VISTA antibody (Fig. 19) resulted in a significant reduction in the tumor size and tumor weight (Fig. 19B-D) which was associated with an increase in the spleen weight (Fig 19E and 19F) and an increase in the frequency of CD8$^+$ T cells (Fig. 19G) without any change in the frequency of CD4$^+$ T cells, NK cells and CD11b$^+$ cells (data not shown). Interestingly, I observed that CD8$^+$ T cells in DKO mice treated with the anti-VISTA antibody expressed significantly higher levels of perforin and GzmB in the TME and spleen (Fig. 19H). Moreover, I noted higher expression of Ki67, TNF-α and IFN-γ expression in CD11b$^+$ cells of DKO mice treated with the anti-VISTA antibody (S. Fig. 10A). Finally, I treated VISTA KO mice with curdlan according to the timelines described in S. Fig. 7A. However, curdlan treatment had no

significant impact on the tumor size (S. Fig. 10 B and C) and spleen size in VISTA KO mice (S. Fig. 10D and E). Although curdlan treatment significantly increased the proportion of $CD11b^{+}$ cells in the TME and spleen, it was at the expense of a reduction in $CD8^{+}$ T cells frequency (S. Fig. 10F and 10G). Furthermore, I noted that $CD8^{+}$ T cells in DKO treated mice with curdlan exhibited reduced perforin and GzmB expression (S. Fig. 10H).

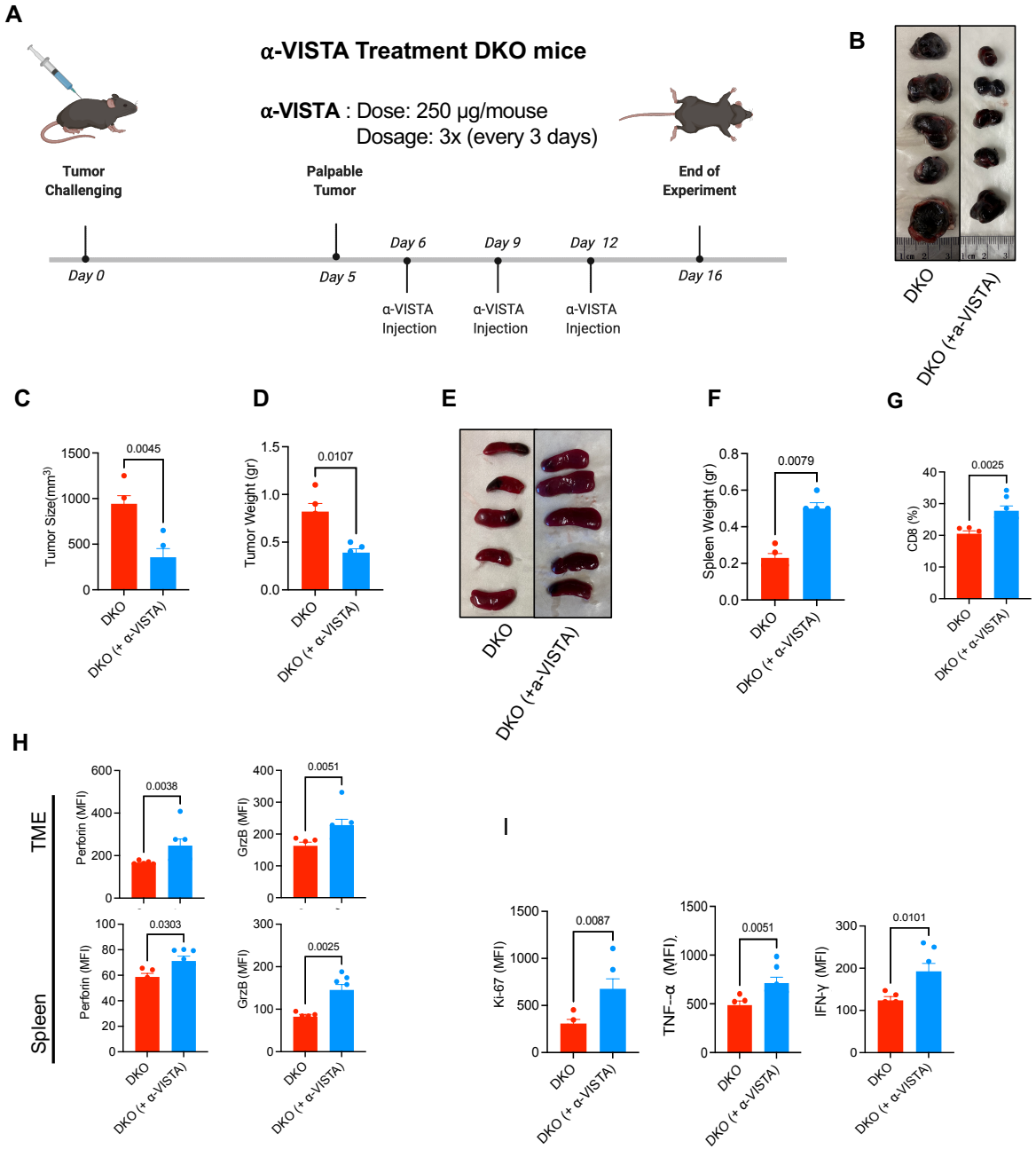

Fig 19. anti-VISTA antibody treated DKO tumor-bearing mice show significant tumor shrinkage. (**A**) Schematic picture of treatment schedule for DKO tumor-bearing mice with α-VISTA monoclonal antibody. (**B**) Representative pictures of dissected tumor tissues from DKO tumor-bearing mice vs DKO plus α-VISTA antibody treated tumor-bearing mice. (**C**) Cumulative data of tumor size in DKO tumor-bearing mice vs DKO plus α-VISTA antibody treated tumor-bearing mice. (**D**) Cumulative data of tumor weight in DKO tumor-bearing mice vs DKO plus α-VISTA antibody treated tumor-bearing mice. (**E**) Representative pictures of dissected spleens from DKO tumor-bearing mice and DKO plus α-VISTA antibody treated tumor-bearing mice. (**F**) Cumulative data of spleen weight in DKO tumor-bearing mice vs DKO plus α-VISTA antibody treated tumor-bearing mice. (**G**) Cumulative data of the frequency of $CD8^+$ T cells among DKO and α-VISTA treated DKO tumor-bearing mice in the TME. (**H**) Cumulative data of the MFI for GrzB and Perforin in tumoral and splenic $CD8^+$ T cells among DKO and α-VISTA treated DKO tumor-bearing mice. (**I**) Cumulative data comparing the MFI of TNF-α, IFN-γ and Ki-67 of tumoral $CD11b^+$ myeloid cells among DKO and α-VISTA treated DKO tumor-bearing mice.

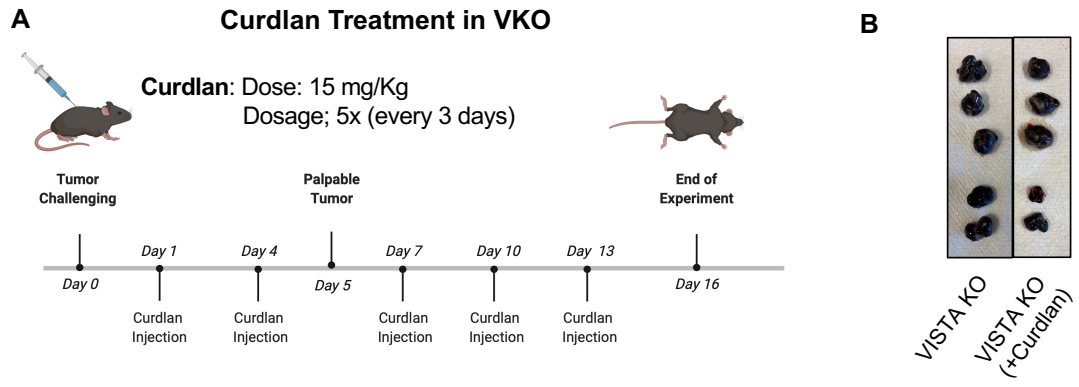
A
Curdlan Treatment in VKO
Curdlan: Dose: 15 mg/Kg
Dosage; 5x (every 3 days)
Tumor Challenging
Palpable Tumor
End of Experiment
Day 0
Day 1
Day 4
Day 5
Day 7
Day 10
Day 13
Day 16
Curdlan Injection
B
VISTA KO
VISTA KO (+Curdlan)

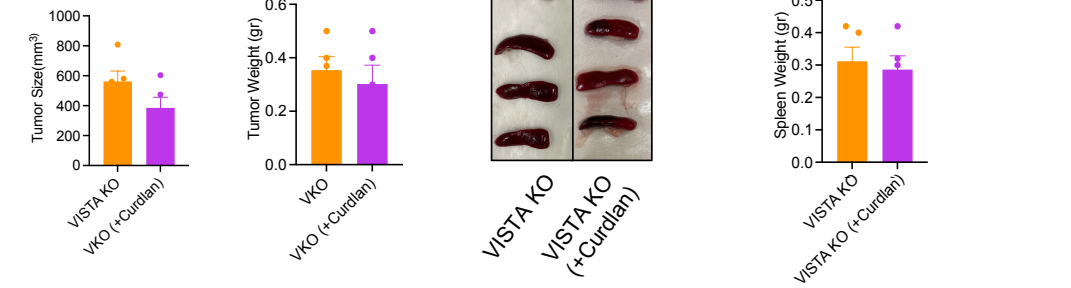
C
Tumor Size(mm3)
VISTA KO
VKO (+Curdlan)
D
Tumor Weight (gr)
VKO
VKO (+Curdlan)
E
VISTA KO
VISTA KO (+Curdlan)
F
Spleen Weight (gr)
VISTA KO
VISTA KO (+Curdlan)

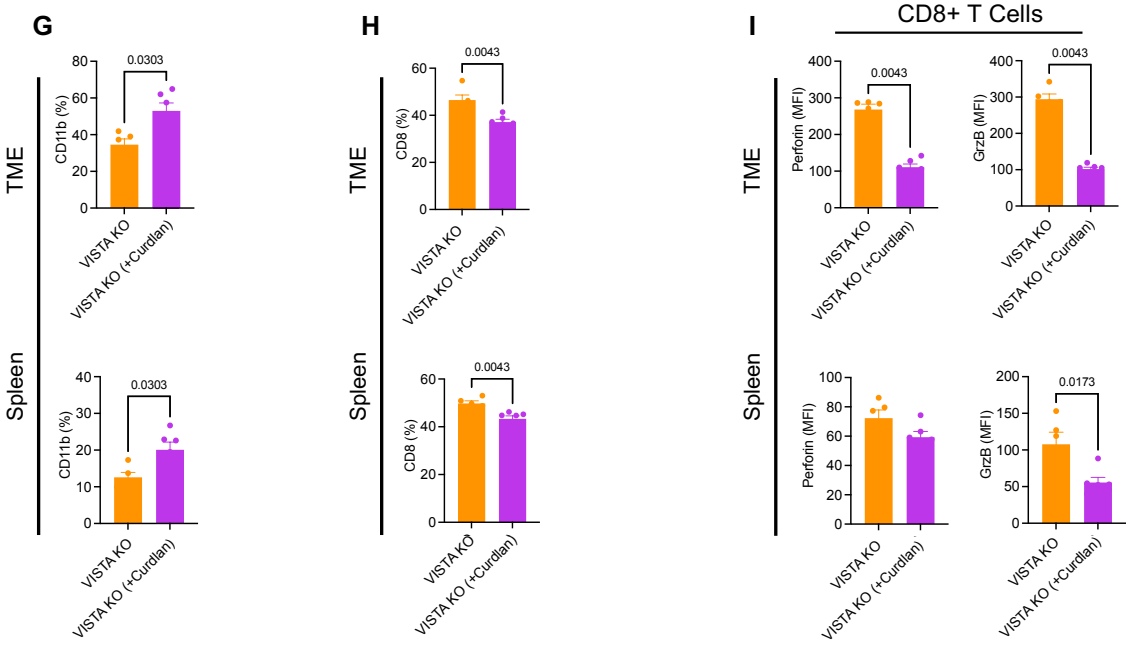
G
TME
Spleen
CD11b (%)
0.0303
VISTA KO
VISTA KO (+Curdlan)
H
CD8 (%)
0.0043
I
CD8+ T Cells
Perforin (MFI)
GrzB (MFI)
0.0173

Fig 20. Curdlan treatment in treated VISTA KO mice didn't improve immune responses. **A**) Schematic picture of treatment schedule for VISTA KO tumor-bearing mice with curdlan. (**B**) Representative pictures of dissected tumor tissues from VISTA KO tumor-bearing mice vs curdlan treated tumor-bearing mice. (**C**) Cumulative data of tumor size in DKO tumor-bearing mice vs DKO plus α-VISTA antibody treated tumor-bearing mice. (**D**) Cumulative data of tumor weight in VISTA KO tumor-bearing mice vs VISTA KO curdlan-treated tumor-bearing mice. (**E**) Representative pictures of dissected spleens from VISTA KO tumor-bearing mice vs VISTA KO curdlan-treated (**F**) Cumulative data of spleen weight in VISTA KO tumor-bearing mice vs VISTA KO curdlan-treated. (**G**) Cumulative data of the frequency of tumoral and splenic $CD11b^+$ myeloid cells in VISTA KO and curdlan-treated VISTA KO tumor-bearing mice. (**H**) Cumulative data of the frequency of tumoral and splenic $CD8^+$ T cells in VISTA KO and curdlan-treated VISTA KO tumor-bearing mice. (**I**) Cumulative data of the MFI for perforin and GrzB in tumoral and splenic $CD8^+$ in VISTA KO and curdlan-treated VISTA KO tumor-bearing mice.

Discussion

Targeting the TME is increasingly considered as a promising approach for cancer therapy (88). Although using ICIs as mono or combination therapies (e.g. PD-1/PDL-1 and CTLA-4) have shown promising results in a few types of cancers, success requires a deeper understanding of the TME and factors that can be targeted to enhance antitumor immune responses. The innate immune cells including DCs, tissue-resident macrophages, and recruited monocytes play an essential role in enhancing or impairing anti-tumor immune responses(89). Recent pieces of evidences suggest that targeting innate immune cells in the TME is an alternative approach for effective anti-tumor immunity (90)(91)(92). In this study, I focused on Dectin-1^+ expressing cells in the TME and periphery of CT26 and B16-F10 tumor models. I also examined the potency of targeting Dectin-1 as a complementary target in the combined immunotherapy setting. I found that the least immunogenic tumor model, B16-F10, had significantly higher proportion of Dectin-1 expressing myeloid cells in the TME than the CT26 tumor model, which is considered an immunogenic model(93). Considering that the frequency of Dectin-1^+ myeloid cells in the TME was negatively correlated with T cell infiltration suggest that higher abundance of Dectin-1^+ myeloid cells might be considered as a hallmark of non-immunogenic tumors. In agreement, Dectin-1 expression by clear cell renal cell carcinoma is reported to be associated with adverse postoperative prognosis(78). Mechanistically the interaction of Dectin-1 with Gal-9 results in tolerogenic macrophage programming and adaptive immune system impairment, which accelerates tumor progression in PDA model (54). However, my observations may not support a crucial role for Gal-

9 in B16-F10 and CT26 tumor models because its expression on tumor cells was negligible. More importantly, I observed a small portion of myeloid cells in the TME and spleen expressing Gal-9. However, I found that myeloid cells in the TME but not spleen and peripheral blood profoundly expressed Dectin-1, which was more significant at the protein and gene levels in the B16-F10 versus the CT26 model. These results are consistent by another report showing that this molecule was predominantly expressed by different myeloid subsets, including macrophages, monocytes and neutrophils(79). In particular, I noted a differential expression of Dectin-1 in different subsets of myeloid cells in the TME. This implies that Dectin-1 may exhibit different roles in different myeloid subsets in the TME. For example, it is reported that yeast-derived particulate β-Glucan via ligation with Dectin-1 induces apoptosis in G-MDSCs but promotes the maturation of M-MDSCs (94).

Dectin-1 is an activation receptor that can stimulate immune cell maturation and enhance cytokines and chemokines production (95). As Dectin-1 was found predominantly on tumor cells in my study, tumor cells might get activated through this signal and influence the immunoregulatory network of the TME. Although I was unable to identify the mechanism(s) underlying the upregulation of Dectin-1 on myeloid and tumor cells, it is reported that macrophages treated with IL-4 and IL-13 upregulate the expression of Dectin-1 and IL-10 expressing APC in human express high levels of Dectin-1 (96)(97). Furthermore, it is recently reported that anti-inflammatory macrophages in small intestine expressed high levels of Dectin-1(98). Therefore, the cytokine milieu of the TME might be a potential factor in Dectin-1 upregulation on immune and non-immune cells. The TME hosts a heterogeneous population of myeloid cells with different dynamics and plasticity. In my research, however, Dectin-1 expression was predominantly associated with an activated myeloid cell phenotype in the TME as characterized by the expression of CD80, CD86 and I-A/I-E. It is possible to speculate that overexpression of antigen presentation molecules (e.g. MHC-I and II) and co-stimulatory molecules (e.g. CD80 and CD86) can enhance anti-tumor immune response (99)(100). Nevertheless, I did not observe a clear picture to support functional properties of Dectin-1^+ myeloid cells. It appears that Dectin-1^+ myeloid cells exhibit an anti-inflammatory profile in the B16-F10 model evidenced by the higher expression of Arg-I and ROS in the TME but a mixed phenotype in the B16-F10 tumor mode. It is worth mentioning that Arg-I and Arg-II hydrolyze L-arginine, a dibasic cationic amino acid, to L-ornithine and play an important immunosuppressive role in the TME(101). In humans, arginine deprivation inhibits T

cell proliferation through decreasing CD3ζ-chain expression and prevents the cycle regulators cyclinD3 and cdk4 (102). Hence, a higher expression of Arg-I by Dectin-1 expressing myeloid cells suggests that these cells may exhibit an inhibitory signal and suppression of Arg-1 could amplify the adaptive immune response in the TME (103). ROS is another immunomodulatory component of the TME, primary resealed by myeloid cells, tumor cells and tumor-associated fibroblasts, which triggers genome-wide DNA mutation, tumorigenesis, angiogenesis, and metastasis (104)(105)(106). ROS depending on the cancer type and its concentration could act as a stimulatory or an inhibitory molecule. It is well-known that lower concentration of ROS is necessary for regulation of cell signalling and induction of respiratory burst in myeloid cells(107). By analysis the ROS expression by Dectin-1^+ myeloid cells in CT26 and B16-F10 tumor models, I found that myeloid cells in the latter model produced a significant amount of this molecule. It is possible to speculate that lower ROS expression in Dectin-1^+ myeloid cells in CT26 may reduce ROS-mediated cell death in colon cancer (108). In contrast, higher expression of ROS in the B16-F10 model may enhance DNA damage and supress immune responses(109)(110)(111). Obviously, further in deep analysis will be required to better characterize the functional properties of cancer-induced Dectin-1^+ myeloid cells in different cancer types.

Examination of the TME Dectin-1^+ myeloid cells revealed that this subset extensively expresses PDL-1, VISTA, PDL-2, TIM-3 and Gal-9. The expression of co-inhibitory receptors is regarded as the hallmark of T cell exhaustion and blockade of immune checkpoints (e.g. PD-1/PD-L1 and CTLA-4) has achieved considerable success in the treatment of different solid cancers(112). Hence, Dectin-1^+ myeloid cells by possessing elevated levels of co-inhibitory receptors/ligands might exhibit a broader role in immune regulation in the TME. One of the most significant observations in this study is the discovery of Dectin-1/VISTA and Dectin-1/PDL-1 co-expression and co-localization in myeloid cells from the TME. These results indicate a novel mechanism beyond the Dectin-1 signaling in modulating T cell plasticity in the TME. For example, Dectin-1^+ myeloid cells may via PD-L-1/PDL-2 suppress PD-1 expressing T cells in the TME (112). Similarly, Gal-9 ligation with TIM-3 can induce an inhibitory signal and has been considered to be an exhaustion mechanism for antigen-specific $CD8^+$ T cells(113)(114). Moreover, recent studies have revealed that Gal-9 interaction with PD-1 and Gal-9 expressing T cell exhibit an impaired phenotype(77)(115)(116)(117). Of note, Gal-9 interacts with different receptors and its interaction with Dectin-1 experts an inhibitory effect to Dectin-1 signaling, which promotes

pancreatic carcinoma (54). Another important observation of this study is the discovery of profound Dectin-1 and VISTA co-expression on myeloid cells not only in the TME but also the spleen of tumor-bearing mice. Although the expression of VISTA on myeloid cells and regulatory T cells in the TME has been reported (118), co-expression of Dectin-1 and VISTA has never been documented. VISTA is a unique co-inhibitory molecules among other immunoglobulin superfamily molecules since it lacks classic immunoreceptor tyrosine-based inhibitory motif (ITIM) or immunoreceptor tyrosine-based switch motifs (ITSM) (119)(120). This may explain dual role for VISTA on myeloid cells or T cells as a ligand or receptor, respectively. The inhibitory function of VISTA has widely been studied in cancer models (121)(122)(123)(86)(124)(125)(126). For instance, VISTA inhibits the activation of MAP kinases and NF-κB signalling cascades and blocking VISTA amplifies TLR/MyD88-mediated pathway in myeloid cells(31). Given that VISTA and PDL-1 were highly co-expressed with Dectin-1 in myeloid cells of B16-F10 model, I postulated that Dectin-1 may enhance tumor progression. Surprisingly, I found that DKO mice had impaired immune cell activation and infiltration into the TME. This is in contrast to a report showing a tolerogenic role for Dectin-1 signaling in PDA(54). However, I found that stimulation of Dectin-1 by curdlan enhanced anti-tumor immunity and reduced tumor progression. Additional evidence support my observations that Dectin-1 stimulation on myeloid cells is essential to NK-cell-mediated tumor cytotoxicity(67). It is reported that Dectin-1 activation in this model results in the activation of the interferon regulatory factor 5 transcriptional factor and downstream gene associated with enhanced NK cell tumoricidal activity(67). Also, Dectin-1 ligation with β -glucan has been reported to confer protection against lung and mammary tumors in mice(127). Similarly, studies in human subjects support a protective role for Dectin-1 signaling against cancer (128)(129). Interestingly, I found that Dectin-1 expressing myeloid cells were enriched in the tumor periphery. Therefore, targeting these cells might be more accessible from the therapeutic standpoint, which can overall enhance anti-tumor immunity. Beyond discovering a protective significant role for Dectin-1 signaling in myeloid cells in the TME, one of the most exciting findings in my study is the downregulation of PDL-1 and VISTA upon curdlan-induced myeloid cells activation. Thus, these data might have far-reaching implications that imply a wider role for targeting Dectin-1 in the TME. Although VISTA KO mice exhibited a robust anti-tumor immune response against tumor, which is in agreement with other reports(118)(86), ligation of Dectin-1 with curdlan did not influence the tumor growth in these

mice. Therefore, further studies are required to test different treatment regiments to determine whether combining dietary β-glucan structures alongside anti-VISTA and/or anti-PDL-1 antibodies enhance anti-tumor immune responses.

Moreover, I found a subset of Dectin-1 expressing T cells, mainly $CD4^+$ T cells, in the TME. It is worth mentioning that these cells were more abundant in the TME of the B16-F10 model. In contrast to a previous report(85), my results show that Dectin-1^+ T cells are heterogeneous but express substantial levels of co-inhibitory receptors. Although upregulation of co-inhibitory receptors is the hallmark of T cell exhaustion, I found that Dectin-1^+ T cells did not exhibit such phenotype. This might be due to the nature of my studies that terminated by 16 days. These observations suggest that these T cells could be targeted by curdlan like myeloid cells. However, further studies are needed to better characterize effector functions of Dectin-1^+ T cells in other animal tumor models and human cancers. My findings highlight the complex network of immunosuppressive pathways present in the TME that is unlikely to be overcome with a single immunotherapy target. Therefore, in addition to ICIs, Dectin-1 would be an attractive target for future immunotherapy development. Stimulation of Dectin-1 may polarize M2 macrophages into an M1-phenotype (68) likely to have synergistic efficacy with ICIs. It is conceivable that Dectin-1^+ $CD8^+$ T cells expressing co-inhibitory receptors eventually become exhausted in the context of chronic conditions. Taken together, stimulating myeloid cells via curdlan not only enhances antigen presentation but also reprograms tumor-associate myeloid cells toward an inflammatory phenotype. This is highly important for melanoma patients because acquired resistance to ICIs is associated with defects in antigen presentation(130). Therefore, targeting Dectin-1 (e.g. curdlan) can result in a robust innate and adaptive immune responses against tumor cells. In agreement with my results, a study suggested that durable regression of melanoma tumors requires concurrent immunotherapy that engages both innate and adaptive immune responses(131). However, there are several limitations in my study, one of which is single-centred treatment design. Also, because of the animal ethics requirements I was unable to keep tumor-bearing mice for a longer period to determine the role of targeting Dectin-1 in a more chronic condition. Moreover, I was unable to investigate the detailed role of Dectin-1 expressing myeloid and T cells in the TME, which merits further investigations.

Works Cited

1. McCarthy EF. The toxins of William B. Coley and the treatment of bone and soft-tissue sarcomas. Iowa Orthop J [Internet]. 2006;26:154–8. Available from: https://pubmed.ncbi.nlm.nih.gov/16789469
2. Rosenberg SA, Mulé JJ, Spiess PJ, Reichert CM, Schwarz SL. Regression of established pulmonary metastases and subcutaneous tumor mediated by the systemic administration of high-dose recombinant interleukin 2. J Exp Med [Internet]. 1985 May 1;161(5):1169–88. Available from: https://pubmed.ncbi.nlm.nih.gov/3886826
3. Rosenberg SA, Lotze MT, Muul LM, Leitman S, Chang AE, Ettinghausen SE, et al. Observations on the Systemic Administration of Autologous Lymphokine-Activated Killer Cells and Recombinant Interleukin-2 to Patients with Metastatic Cancer. N Engl J Med [Internet]. 1985 Dec 5;313(23):1485–92. Available from: https://doi.org/10.1056/NEJM198512053132327
4. Waldmann TA. Cytokines in Cancer Immunotherapy. Cold Spring Harb Perspect Biol [Internet]. 2018 Dec 3;10(12):a028472. Available from: https://pubmed.ncbi.nlm.nih.gov/29101107
5. Ferrantini M, Capone I, Belardelli F. Interferon-α and cancer: Mechanisms of action and new perspectives of clinical use. Biochimie [Internet]. 2007;89(6):884–93. Available from: https://www.sciencedirect.com/science/article/pii/S0300908407001010
6. Baldo BA. Side effects of cytokines approved for therapy. Drug Saf [Internet]. 2014 Nov;37(11):921–43. Available from: https://pubmed.ncbi.nlm.nih.gov/25270293
7. Vial T, Descotes J. Immune-mediated side-effects of cytokines in humans. Toxicology [Internet]. 1995;105(1):31–57. Available from: https://www.sciencedirect.com/science/article/pii/0300483X9503124X
8. Saxena M, van der Burg SH, Melief CJM, Bhardwaj N. Therapeutic cancer vaccines. Nat Rev Cancer [Internet]. 2021;21(6):360–78. Available from: https://doi.org/10.1038/s41568-021-00346-0
9. Pardi N, Hogan MJ, Porter FW, Weissman D. mRNA vaccines - a new era in vaccinology. Nat Rev Drug Discov [Internet]. 2018/01/12. 2018 Apr;17(4):261–79. Available from: https://pubmed.ncbi.nlm.nih.gov/29326426
10. Miao L, Zhang Y, Huang L. mRNA vaccine for cancer immunotherapy. Mol Cancer [Internet]. 2021;20(1):41. Available from: https://doi.org/10.1186/s12943-021-01335-5
11. Zhao Y, Baldin A V, Isayev O, Werner J, Zamyatnin Jr AA, Bazhin A V. Cancer Vaccines: Antigen Selection Strategy. Vaccines [Internet]. 2021 Jan 25;9(2):85. Available from: https://pubmed.ncbi.nlm.nih.gov/33503926
12. Palucka K, Banchereau J. Dendritic-cell-based therapeutic cancer vaccines. Immunity [Internet]. 2013 Jul 25;39(1):38–48. Available from: https://pubmed.ncbi.nlm.nih.gov/23890062
13. Santos PM, Butterfield LH. Dendritic Cell-Based Cancer Vaccines. J Immunol [Internet]. 2018 Jan 15;200(2):443–9. Available from: https://pubmed.ncbi.nlm.nih.gov/29311386
14. Shi T, Song X, Wang Y, Liu F, Wei J. Combining Oncolytic Viruses With Cancer Immunotherapy: Establishing a New Generation of Cancer Treatment [Internet]. Vol. 11, Frontiers in Immunology . 2020. p. 683. Available from: https://www.frontiersin.org/article/10.3389/fimmu.2020.00683
15. Baxevanis CN, Fortis SP, Ardavanis A, Perez SA. Exploring Essential Issues for Improving Therapeutic Cancer Vaccine Trial Design. Cancers (Basel) [Internet]. 2020 Oct

10;12(10):2908. Available from: https://pubmed.ncbi.nlm.nih.gov/33050520
16. Donninger H, Li C, Eaton JW, Yaddanapudi K. Cancer Vaccines: Promising Therapeutics or an Unattainable Dream. Vaccines [Internet]. 2021 Jun 18;9(6):668. Available from: https://pubmed.ncbi.nlm.nih.gov/34207062
17. Hollingsworth RE, Jansen K. Turning the corner on therapeutic cancer vaccines. npj Vaccines [Internet]. 2019;4(1):7. Available from: https://doi.org/10.1038/s41541-019-0103-y
18. Lim J, Park Y, Ahn JW, Sim J, Kang SJ, Hwang S, et al. Autologous adoptive immune-cell therapy elicited a durable response with enhanced immune reaction signatures in patients with recurrent glioblastoma: An open label, phase I/IIa trial. PLoS One [Internet]. 2021 Mar 10;16(3):e0247293–e0247293. Available from: https://pubmed.ncbi.nlm.nih.gov/33690665
19. Morotti M, Albukhari A, Alsaadi A, Artibani M, Brenton JD, Curbishley SM, et al. Promises and challenges of adoptive T-cell therapies for solid tumours. Br J Cancer [Internet]. 2021;124(11):1759–76. Available from: https://doi.org/10.1038/s41416-021-01353-6
20. Papadopoulou* ANM and LC. CAR T-cell Therapy: A New Era in Cancer Immunotherapy [Internet]. Vol. 19, Current Pharmaceutical Biotechnology. 2018. p. 5–18. Available from: http://www.eurekaselect.com/node/161365/article
21. Hou AJ, Chen LC, Chen YY. Navigating CAR-T cells through the solid-tumour microenvironment. Nat Rev Drug Discov [Internet]. 2021;20(7):531–50. Available from: https://doi.org/10.1038/s41573-021-00189-2
22. Sterner RC, Sterner RM. CAR-T cell therapy: current limitations and potential strategies. Blood Cancer J [Internet]. 2021;11(4):69. Available from: https://doi.org/10.1038/s41408-021-00459-7
23. Tang H, Qiao J, Fu Y-X. Immunotherapy and tumor microenvironment. Cancer Lett [Internet]. 2015/10/19. 2016 Jan 1;370(1):85–90. Available from: https://pubmed.ncbi.nlm.nih.gov/26477683
24. Carlson RD, Flickinger Jr JC, Snook AE. Talkin' Toxins: From Coley's to Modern Cancer Immunotherapy. Toxins (Basel) [Internet]. 2020 Apr 9;12(4):241. Available from: https://pubmed.ncbi.nlm.nih.gov/32283684
25. Zhao L, Cao YJ. Engineered T Cell Therapy for Cancer in the Clinic. Front Immunol [Internet]. 2019;10:2250. Available from: https://www.frontiersin.org/article/10.3389/fimmu.2019.02250
26. Robert C. A decade of immune-checkpoint inhibitors in cancer therapy. Nat Commun [Internet]. 2020;11(1):3801. Available from: https://doi.org/10.1038/s41467-020-17670-y
27. Nakamura K, Smyth MJ. Myeloid immunosuppression and immune checkpoints in the tumor microenvironment. Cell Mol Immunol [Internet]. 2020;17(1):1–12. Available from: https://doi.org/10.1038/s41423-019-0306-1
28. Robert C, Schachter J, Long G V, Arance A, Grob JJ, Mortier L, et al. Pembrolizumab versus Ipilimumab in Advanced Melanoma. N Engl J Med [Internet]. 2015 Apr 19;372(26):2521–32. Available from: https://doi.org/10.1056/NEJMoa1503093
29. Hamid O, Robert C, Daud A, Hodi FS, Hwu W-J, Kefford R, et al. Safety and Tumor Responses with Lambrolizumab (Anti–PD-1) in Melanoma. N Engl J Med [Internet]. 2013 Jun 2;369(2):134–44. Available from: https://doi.org/10.1056/NEJMoa1305133
30. Strauss L, Mahmoud MAA, Weaver JD, Tijaro-Ovalle NM, Christofides A, Wang Q, et

al. Targeted deletion of PD-1 in myeloid cells induces antitumor immunity. Sci Immunol [Internet]. 2020 Jan 3;5(43):eaay1863. Available from: https://pubmed.ncbi.nlm.nih.gov/31901074
31. Xu W, Dong J, Zheng Y, Zhou J, Yuan Y, Ta HM, et al. Immune-Checkpoint Protein VISTA Regulates Antitumor Immunity by Controlling Myeloid Cell–Mediated Inflammation and Immunosuppression. Cancer Immunol Res [Internet]. 2019 Sep 1;7(9):1497 LP – 1510. Available from: http://cancerimmunolres.aacrjournals.org/content/7/9/1497.abstract
32. Martins F, Sofiya L, Sykiotis GP, Lamine F, Maillard M, Fraga M, et al. Adverse effects of immune-checkpoint inhibitors: epidemiology, management and surveillance. Nat Rev Clin Oncol [Internet]. 2019;16(9):563–80. Available from: https://doi.org/10.1038/s41571-019-0218-0
33. Haslam A, Prasad V. Estimation of the Percentage of US Patients With Cancer Who Are Eligible for and Respond to Checkpoint Inhibitor Immunotherapy Drugs. JAMA Netw Open [Internet]. 2019 May 3;2(5):e192535–e192535. Available from: https://doi.org/10.1001/jamanetworkopen.2019.2535
34. Johnson DB, Rioth MJ, Horn L. Immune checkpoint inhibitors in NSCLC. Curr Treat Options Oncol [Internet]. 2014 Dec;15(4):658–69. Available from: https://pubmed.ncbi.nlm.nih.gov/25096781
35. Bai R, Lv Z, Xu D, Cui J. Predictive biomarkers for cancer immunotherapy with immune checkpoint inhibitors. Biomark Res [Internet]. 2020;8(1):34. Available from: https://doi.org/10.1186/s40364-020-00209-0
36. Vafaizadeh V, Barekati Z. Immuno-Oncology Biomarkers for Personalized Immunotherapy in Breast Cancer. Front Cell Dev Biol [Internet]. 2020;8:162. Available from: https://www.frontiersin.org/article/10.3389/fcell.2020.00162
37. Yang Y, Li C, Liu T, Dai X, Bazhin A V. Myeloid-Derived Suppressor Cells in Tumors: From Mechanisms to Antigen Specificity and Microenvironmental Regulation [Internet]. Vol. 11, Frontiers in Immunology . 2020. p. 1371. Available from: https://www.frontiersin.org/article/10.3389/fimmu.2020.01371
38. Veglia F, Sanseviero E, Gabrilovich DI. Myeloid-derived suppressor cells in the era of increasing myeloid cell diversity. Nat Rev Immunol [Internet]. 2021;21(8):485–98. Available from: https://doi.org/10.1038/s41577-020-00490-y
39. Wu L, Zhang XH-F. Tumor-Associated Neutrophils and Macrophages—Heterogenous but Not Chaotic [Internet]. Vol. 11, Frontiers in Immunology . 2020. p. 3117. Available from: https://www.frontiersin.org/article/10.3389/fimmu.2020.553967
40. Lin Y, Xu J, Lan H. Tumor-associated macrophages in tumor metastasis: biological roles and clinical therapeutic applications. J Hematol Oncol [Internet]. 2019;12(1):76. Available from: https://doi.org/10.1186/s13045-019-0760-3
41. Li D, Wu M. Pattern recognition receptors in health and diseases. Signal Transduct Target Ther [Internet]. 2021;6(1):291. Available from: https://doi.org/10.1038/s41392-021-00687-0
42. Amarante-Mendes GP, Adjemian S, Branco LM, Zanetti LC, Weinlich R, Bortoluci KR. Pattern Recognition Receptors and the Host Cell Death Molecular Machinery [Internet]. Vol. 9, Frontiers in Immunology . 2018. p. 2379. Available from: https://www.frontiersin.org/article/10.3389/fimmu.2018.02379
43. Gordon S. Pattern Recognition Receptors: Doubling Up for the Innate Immune Response.

Cell [Internet]. 2002 Dec 27;111(7):927–30. Available from: https://doi.org/10.1016/S0092-8674(02)01201-1
44. Shekarian T, Valsesia-Wittmann S, Brody J, Michallet MC, Depil S, Caux C, et al. Pattern recognition receptors: immune targets to enhance cancer immunotherapy. Ann Oncol [Internet]. 2017 Aug 1;28(8):1756–66. Available from: https://doi.org/10.1093/annonc/mdx179
45. Patel SA, Minn AJ. Combination Cancer Therapy with Immune Checkpoint Blockade: Mechanisms and Strategies. Immunity [Internet]. 2018 Mar 20;48(3):417–33. Available from: https://pubmed.ncbi.nlm.nih.gov/29562193
46. Chuang Y-C, Tseng J-C, Huang L-R, Huang C-M, Huang C-YF, Chuang T-H. Adjuvant Effect of Toll-Like Receptor 9 Activation on Cancer Immunotherapy Using Checkpoint Blockade [Internet]. Vol. 11, Frontiers in Immunology . 2020. p. 1075. Available from: https://www.frontiersin.org/article/10.3389/fimmu.2020.01075
47. Gombault A, Baron L, Couillin I. ATP release and purinergic signaling in NLRP3 inflammasome activation. Front Immunol [Internet]. 2013 Jan 8;3:414. Available from: https://pubmed.ncbi.nlm.nih.gov/23316199
48. Pandey S, Singh S, Anang V, Bhatt AN, Natarajan K, Dwarakanath BS. Pattern Recognition Receptors in Cancer Progression and Metastasis. Cancer Growth Metastasis [Internet]. 2015 Jul 23;8:25–34. Available from: https://pubmed.ncbi.nlm.nih.gov/26279628
49. Urban-Wojciuk Z, Khan MM, Oyler BL, Fåhraeus R, Marek-Trzonkowska N, Nita-Lazar A, et al. The Role of TLRs in Anti-cancer Immunity and Tumor Rejection. Front Immunol [Internet]. 2019;10:2388. Available from: https://www.frontiersin.org/article/10.3389/fimmu.2019.02388
50. Huang B, Zhao J, Unkeless JC, Feng ZH, Xiong H. TLR signaling by tumor and immune cells: a double-edged sword. Oncogene [Internet]. 2008;27(2):218–24. Available from: https://doi.org/10.1038/sj.onc.1210904
51. Chiffoleau E. C-Type Lectin-Like Receptors As Emerging Orchestrators of Sterile Inflammation Represent Potential Therapeutic Targets. Front Immunol [Internet]. 2018 Feb 15;9:227. Available from: https://pubmed.ncbi.nlm.nih.gov/29497419
52. Geijtenbeek TBH, Gringhuis SI. Signalling through C-type lectin receptors: shaping immune responses. Nat Rev Immunol [Internet]. 2009;9(7):465–79. Available from: https://doi.org/10.1038/nri2569
53. Mayer S, Raulf M-K, Lepenies B. C-type lectins: their network and roles in pathogen recognition and immunity. Histochem Cell Biol [Internet]. 2017;147(2):223–37. Available from: https://doi.org/10.1007/s00418-016-1523-7
54. Daley D, Mani VR, Mohan N, Akkad N, Ochi A, Heindel DW, et al. Dectin 1 activation on macrophages by galectin 9 promotes pancreatic carcinoma and peritumoral immune tolerance. Nat Med. 2017;
55. Kiyotake R, Oh-Hora M, Ishikawa E, Miyamoto T, Ishibashi T, Yamasaki S. Human Mincle Binds to Cholesterol Crystals and Triggers Innate Immune Responses. J Biol Chem [Internet]. 2015/08/20. 2015 Oct 16;290(42):25322–32. Available from: https://pubmed.ncbi.nlm.nih.gov/26296894
56. Zheng D, Liwinski T, Elinav E. Interaction between microbiota and immunity in health and disease. Cell Res [Internet]. 2020;30(6):492–506. Available from: https://doi.org/10.1038/s41422-020-0332-7

57. Willment JA, Marshall ASJ, Reid DM, Williams DL, Wong SYC, Gordon S, et al. The human β-glucan receptor is widely expressed and functionally equivalent to murine Dectin-1 on primary cells. Eur J Immunol [Internet]. 2005;35(5):1539–47. Available from: https://onlinelibrary.wiley.com/doi/abs/10.1002/eji.200425725
58. Heinsbroek SEM, Taylor PR, Rosas M, Willment JA, Williams DL, Gordon S, et al. Expression of Functionally Different Dectin-1 Isoforms by Murine Macrophages. J Immunol [Internet]. 2006;176(9):5513–8. Available from: https://www.jimmunol.org/content/176/9/5513
59. Kalia N, Singh J, Kaur M. The role of dectin-1 in health and disease. Immunobiology [Internet]. 2021;226(2):152071. Available from: https://www.sciencedirect.com/science/article/pii/S017129852100019X
60. Underhill DM, Rossnagle E, Lowell CA, Simmons RM. Dectin-1 activates Syk tyrosine kinase in a dynamic subset of macrophages for reactive oxygen production. Blood [Internet]. 2005/06/14. 2005 Oct 1;106(7):2543–50. Available from: https://pubmed.ncbi.nlm.nih.gov/15956283
61. Herre J, Marshall ASJ, Caron E, Edwards AD, Williams DL, Schweighoffer E, et al. Dectin-1 uses novel mechanisms for yeast phagocytosis in macrophages. Blood [Internet]. 2004 Dec 15;104(13):4038–45. Available from: https://doi.org/10.1182/blood-2004-03-1140
62. Dalpke AH, Opper S, Zimmermann S, Heeg K. Suppressors of Cytokine Signaling (SOCS)-1 and SOCS-3 Are Induced by CpG-DNA and Modulate Cytokine Responses in APCs. J Immunol [Internet]. 2001 Jun 15;166(12):7082 LP – 7089. Available from: http://www.jimmunol.org/content/166/12/7082.abstract
63. Eberle ME, Dalpke AH. Dectin-1 Stimulation Induces Suppressor of Cytokine Signaling 1, Thereby Modulating TLR Signaling and T Cell Responses. J Immunol [Internet]. 2012 Jun 1;188(11):5644 LP – 5654. Available from: http://www.jimmunol.org/content/188/11/5644.abstract
64. Redza-Dutordoir M, Averill-Bates DA. Activation of apoptosis signalling pathways by reactive oxygen species. Biochim Biophys Acta - Mol Cell Res [Internet]. 2016;1863(12):2977–92. Available from: https://www.sciencedirect.com/science/article/pii/S0167488916302324
65. Roux C, Jafari SM, Shinde R, Duncan G, Cescon DW, Silvester J, et al. Reactive oxygen species modulate macrophage immunosuppressive phenotype through the up-regulation of PD-L1. Proc Natl Acad Sci [Internet]. 2019 Mar 5;116(10):4326 LP – 4335. Available from: http://www.pnas.org/content/116/10/4326.abstract
66. Brown GD, Gordon S. A new receptor for β-glucans. Nature [Internet]. 2001;413(6851):36–7. Available from: https://doi.org/10.1038/35092620
67. Chiba S, Ikushima H, Ueki H, Yanai H, Kimura Y, Hangai S, et al. Recognition of tumor cells by Dectin-1 orchestrates innate immune cells for anti-tumor responses. Elife [Internet]. 2014 Aug 22;3:e04177–e04177. Available from: https://pubmed.ncbi.nlm.nih.gov/25149452
68. Liu M, Luo F, Ding C, Albeituni S, Hu X, Ma Y, et al. Dectin-1 Activation by a Natural Product β-Glucan Converts Immunosuppressive Macrophages into an M1-like Phenotype. J Immunol [Internet]. 2015/10/09. 2015 Nov 15;195(10):5055–65. Available from: https://pubmed.ncbi.nlm.nih.gov/26453753
69. Adams EL, Rice PJ, Graves B, Ensley HE, Yu H, Brown GD, et al. Differential High-

Affinity Interaction of Dectin-1 with Natural or Synthetic Glucans Is Dependent upon Primary Structure and Is Influenced by Polymer Chain Length and Side-Chain Branching. J Pharmacol Exp Ther [Internet]. 2008;325(1):115–23. Available from: https://jpet.aspetjournals.org/content/325/1/115

70. Allavena P, Chieppa M, Bianchi G, Solinas G, Fabbri M, Laskarin G, et al. Engagement of the mannose receptor by tumoral mucins activates an immune suppressive phenotype in human tumor-associated macrophages. Clin Dev Immunol [Internet]. 2011/02/09. 2010;2010:547179. Available from: https://pubmed.ncbi.nlm.nih.gov/21331365
71. Bode K, Bujupi F, Link C, Hein T, Zimmermann S, Peiris D, et al. Dectin-1 Binding to Annexins on Apoptotic Cells Induces Peripheral Immune Tolerance via NADPH Oxidase-2. Cell Rep [Internet]. 2019 Dec 24;29(13):4435-4446.e9. Available from: https://doi.org/10.1016/j.celrep.2019.11.086
72. Mummert ME, Mummert DI, Ellinger L, Takashima A. Functional Roles of Hyaluronan in B16-F10 Melanoma Growth and Experimental Metastasis in Mice¹ Mol Cancer Ther [Internet]. 2003 Mar 1;2(3):295 LP – 300. Available from: http://mct.aacrjournals.org/content/2/3/295.abstract
73. Zhou P, L'italien L, Hodges D, Schebye XM. Pivotal Roles of CD4⁺ Effector T cells in Mediating Agonistic Anti-GITR mAb-Induced-Immune Activation and Tumor Immunity in CT26 Tumors. J Immunol [Internet]. 2007 Dec 1;179(11):7365 LP – 7375. Available from: http://www.jimmunol.org/content/179/11/7365.abstract
74. Rosenbaum SR, Knecht M, Mollaee M, Zhong Z, Erkes DA, McCue PA, et al. FOXD3 Regulates VISTA Expression in Melanoma. Cell Rep [Internet]. 2020 Jan 14;30(2):510-524.e6. Available from: https://pubmed.ncbi.nlm.nih.gov/31940493
75. Zhao Y, Chu X, Chen J, Wang Y, Gao S, Jiang Y, et al. Dectin-1-activated dendritic cells trigger potent antitumour immunity through the induction of Th9 cells. Nat Commun [Internet]. 2016;7(1):12368. Available from: https://doi.org/10.1038/ncomms12368
76. Mashhouri S, Koleva P, Huynh M, Okoye I, Shahbaz S, Elahi S. Sex Matters: Physiological Abundance of Immuno-Regulatory CD71+ Erythroid Cells Impair Immunity in Females [Internet]. Vol. 12, Frontiers in Immunology . 2021. p. 2893. Available from: https://www.frontiersin.org/article/10.3389/fimmu.2021.705197
77. Okoye I, Xu L, Motamedi M, Parashar P, Walker JW, Elahi S. Galectin-9 expression defines exhausted T cells and impaired cytotoxic NK cells in patients with virus-associated solid tumors. J Immunother cancer [Internet]. 2020 Dec;8(2):e001849. Available from: https://pubmed.ncbi.nlm.nih.gov/33310773
78. Xia Y, Liu L, Bai Q, Wang J, Xi W, Qu Y, et al. Dectin-1 predicts adverse postoperative prognosis of patients with clear cell renal cell carcinoma. Sci Rep [Internet]. 2016;6(1):32657. Available from: https://doi.org/10.1038/srep32657
79. Taylor PR, Brown GD, Reid DM, Willment JA, Martinez-Pomares L, Gordon S, et al. The β-Glucan Receptor, Dectin-1, Is Predominantly Expressed on the Surface of Cells of the Monocyte/Macrophage and Neutrophil Lineages. J Immunol [Internet]. 2002 Oct 1;169(7):3876 LP – 3882. Available from: http://www.jimmunol.org/content/169/7/3876.abstract
80. Fan W, Yang X, Huang F, Tong X, Zhu L, Wang S. Identification of CD206 as a potential biomarker of cancer stem-like cells and therapeutic agent in liver cancer. Oncol Lett

[Internet]. 2019/07/26. 2019 Sep;18(3):3218–26. Available from: https://pubmed.ncbi.nlm.nih.gov/31452799
81. Maibach F, Sadozai H, Seyed Jafari SM, Hunger RE, Schenk M. Tumor-Infiltrating Lymphocytes and Their Prognostic Value in Cutaneous Melanoma [Internet]. Vol. 11, Frontiers in Immunology . 2020. p. 2105. Available from: https://www.frontiersin.org/article/10.3389/fimmu.2020.02105
82. Peled M, Onn A, Herbst RS. Tumor-Infiltrating Lymphocytes—Location for Prognostic Evaluation. Clin Cancer Res [Internet]. 2019 Mar 1;25(5):1449 LP – 1451. Available from: http://clincancerres.aacrjournals.org/content/25/5/1449.abstract
83. Schnell A, Schmidl C, Herr W, Siska PJ. The Peripheral and Intratumoral Immune Cell Landscape in Cancer Patients: A Proxy for Tumor Biology and a Tool for Outcome Prediction. Biomedicines [Internet]. 2018 Feb 24;6(1):25. Available from: https://pubmed.ncbi.nlm.nih.gov/29495308
84. Holl EK, Frazier VN, Landa K, Beasley GM, Hwang ES, Nair SK. Examining Peripheral and Tumor Cellular Immunome in Patients With Cancer [Internet]. Vol. 10, Frontiers in Immunology . 2019. p. 1767. Available from: https://www.frontiersin.org/article/10.3389/fimmu.2019.01767
85. Martin B, Hirota K, Cua DJ, Stockinger B, Veldhoen M. Interleukin-17-Producing γδ T Cells Selectively Expand in Response to Pathogen Products and Environmental Signals. Immunity [Internet]. 2009;31(2):321–30. Available from: https://www.sciencedirect.com/science/article/pii/S1074761309003203
86. Liu J, Yuan Y, Chen W, Putra J, Suriawinata AA, Schenk AD, et al. Immune-checkpoint proteins VISTA and PD-1 nonredundantly regulate murine T-cell responses. Proc Natl Acad Sci [Internet]. 2015 May 26;112(21):6682 LP – 6687. Available from: http://www.pnas.org/content/112/21/6682.abstract
87. Wang L, Le Mercier I, Putra J, Chen W, Liu J, Schenk AD, et al. Disruption of the immune-checkpoint VISTA gene imparts a proinflammatory phenotype with predisposition to the development of autoimmunity. Proc Natl Acad Sci [Internet]. 2014 Oct 14;111(41):14846 LP – 14851. Available from: http://www.pnas.org/content/111/41/14846.abstract
88. Shalapour S, Font-Burgada J, Di Caro G, Zhong Z, Sanchez-Lopez E, Dhar D, et al. Immunosuppressive plasma cells impede T-cell-dependent immunogenic chemotherapy. Nature [Internet]. 2015/04/29. 2015 May 7;521(7550):94–8. Available from: https://pubmed.ncbi.nlm.nih.gov/25924065
89. Haas L, Obenauf AC. Allies or Enemies-The Multifaceted Role of Myeloid Cells in the Tumor Microenvironment. Front Immunol [Internet]. 2019 Nov 28;10:2746. Available from: https://pubmed.ncbi.nlm.nih.gov/31849950
90. Demaria O, Cornen S, Daëron M, Morel Y, Medzhitov R, Vivier E. Harnessing innate immunity in cancer therapy. Nature [Internet]. 2019;574(7776):45–56. Available from: https://doi.org/10.1038/s41586-019-1593-5
91. Kather JN, Halama N. Harnessing the innate immune system and local immunological microenvironment to treat colorectal cancer. Br J Cancer [Internet]. 2019;120(9):871–82. Available from: https://doi.org/10.1038/s41416-019-0441-6
92. Corrales L, Matson V, Flood B, Spranger S, Gajewski TF. Innate immune signaling and regulation in cancer immunotherapy. Cell Res [Internet]. 2017;27(1):96–108. Available from: https://doi.org/10.1038/cr.2016.149

93. Lechner MG, Karimi SS, Barry-Holson K, Angell TE, Murphy KA, Church CH, et al. Immunogenicity of murine solid tumor models as a defining feature of in vivo behavior and response to immunotherapy. J Immunother [Internet]. 2013;36(9):477–89. Available from: https://pubmed.ncbi.nlm.nih.gov/24145359
94. Albeituni SH, Ding C, Liu M, Hu X, Luo F, Kloecker G, et al. Yeast-Derived Particulate β-Glucan Treatment Subverts the Suppression of Myeloid-Derived Suppressor Cells (MDSC) by Inducing Polymorphonuclear MDSC Apoptosis and Monocytic MDSC Differentiation to APC in Cancer. J Immunol [Internet]. 2016/01/25. 2016 Mar 1;196(5):2167–80. Available from: https://pubmed.ncbi.nlm.nih.gov/26810222
95. Brown GD. Dectin-1: a signalling non-TLR pattern-recognition receptor. Nat Rev Immunol [Internet]. 2006;6(1):33–43. Available from: https://doi.org/10.1038/nri1745
96. Willment JA, Lin H-H, Reid DM, Taylor PR, Williams DL, Wong SYC, et al. Dectin-1 Expression and Function Are Enhanced on Alternatively Activated and GM-CSF-Treated Macrophages and Are Negatively Regulated by IL-10, Dexamethasone, and Lipopolysaccharide. J Immunol [Internet]. 2003 Dec 1;171(11):6297 LP – 6297. Available from: http://www.jimmunol.org/content/171/11/6297.3.abstract
97. Heine A, Held SAE, Schulte-Schrepping J, Wolff JFA, Klee K, Ulas T, et al. Generation and functional characterization of MDSC-like cells. Oncoimmunology [Internet]. 2017 Feb 23;6(4):e1295203–e1295203. Available from: https://pubmed.ncbi.nlm.nih.gov/28507805
98. Erkelens MN, Goverse G, Konijn T, Molenaar R, Beijer MR, Van den Bossche J, et al. Intestinal Macrophages Balance Inflammatory Expression Profiles via Vitamin A and Dectin-1-Mediated Signaling [Internet]. Vol. 11, Frontiers in Immunology . 2020. Available from: https://www.frontiersin.org/article/10.3389/fimmu.2020.00551
99. Haabeth OAW, Blake TR, McKinlay CJ, Tveita AA, Sallets A, Waymouth RM, et al. Local Delivery of Ox40l, Cd80, and Cd86 mRNA Kindles Global Anticancer Immunity. Cancer Res [Internet]. 2019/01/28. 2019 Apr 1;79(7):1624–34. Available from: https://pubmed.ncbi.nlm.nih.gov/30692215
100. Beyranvand Nejad E, van der Sluis TC, van Duikeren S, Yagita H, Janssen GM, van Veelen PA, et al. Tumor Eradication by Cisplatin Is Sustained by CD80/86-Mediated Costimulation of CD8⁺ T Cells. Cancer Res [Internet]. 2016 Oct 15;76(20):6017 LP – 6029. Available from: http://cancerres.aacrjournals.org/content/76/20/6017.abstract
101. Miret JJ, Kirschmeier P, Koyama S, Zhu M, Li YY, Naito Y, et al. Suppression of Myeloid Cell Arginase Activity leads to Therapeutic Response in a NSCLC Mouse Model by Activating Anti-Tumor Immunity. J Immunother Cancer [Internet]. 2019;7(1):32. Available from: https://doi.org/10.1186/s40425-019-0504-5
102. Rodriguez PC, Quiceno DG, Ochoa AC. L-arginine availability regulates T-lymphocyte cell-cycle progression. Blood [Internet]. 2006/10/05. 2007 Feb 15;109(4):1568–73. Available from: https://pubmed.ncbi.nlm.nih.gov/17023580
103. Thomas AC, Mattila JT. “Of Mice and Men”: Arginine Metabolism in Macrophages [Internet]. Vol. 5, Frontiers in Immunology . 2014. p. 479. Available from: https://www.frontiersin.org/article/10.3389/fimmu.2014.00479
104. Bogdan C, Röllinghoff M, Diefenbach A. Reactive oxygen and reactive nitrogen intermediates in innate and specific immunity. Curr Opin Immunol [Internet]. 2000;12(1):64–76. Available from:

https://www.sciencedirect.com/science/article/pii/S0952791599000527
105. Lambeth JD, Neish AS. Nox Enzymes and New Thinking on Reactive Oxygen: A Double-Edged Sword Revisited. Annu Rev Pathol Mech Dis [Internet]. 2014 Jan 24;9(1):119–45. Available from: https://doi.org/10.1146/annurev-pathol-012513-104651
106. Canli Ö, Nicolas AM, Gupta J, Finkelmeier F, Goncharova O, Pesic M, et al. Myeloid Cell-Derived Reactive Oxygen Species Induce Epithelial Mutagenesis. Cancer Cell [Internet]. 2017;32(6):869-883.e5. Available from: https://www.sciencedirect.com/science/article/pii/S153561081730507X
107. Aboelella NS, Brandle C, Kim T, Ding Z-C, Zhou G. Oxidative Stress in the Tumor Microenvironment and Its Relevance to Cancer Immunotherapy. Cancers (Basel) [Internet]. 2021 Feb 27;13(5):986. Available from: https://pubmed.ncbi.nlm.nih.gov/33673398
108. Coriat R, Marut W, Leconte M, Ba LB, Vienne A, Chéreau C, et al. The organotelluride catalyst LAB027 prevents colon cancer growth in the mice. Cell Death Dis [Internet]. 2011;2(8):e191–e191. Available from: https://doi.org/10.1038/cddis.2011.73
109. Tse AK-W, Chen Y-J, Fu X-Q, Su T, Li T, Guo H, et al. Sensitization of melanoma cells to alkylating agent-induced DNA damage and cell death via orchestrating oxidative stress and IKKβ inhibition. Redox Biol [Internet]. 2017/01/12. 2017 Apr;11:562–76. Available from: https://pubmed.ncbi.nlm.nih.gov/28107677
110. Brand RM, Wipf P, Durham A, Epperly MW, Greenberger JS, Falo LD. Targeting Mitochondrial Oxidative Stress to Mitigate UV-Induced Skin Damage [Internet]. Vol. 9, Frontiers in Pharmacology . 2018. p. 920. Available from: https://www.frontiersin.org/article/10.3389/fphar.2018.00920
111. Wang H-T, Choi B, Tang M. Melanocytes are deficient in repair of oxidative DNA damage and UV-induced photoproducts. Proc Natl Acad Sci [Internet]. 2010 Jul 6;107(27):12180 LP – 12185. Available from: http://www.pnas.org/content/107/27/12180.abstract
112. Okoye IS, Houghton M, Tyrrell L, Barakat K, Elahi S. Coinhibitory Receptor Expression and Immune Checkpoint Blockade: Maintaining a Balance in CD8(+) T Cell Responses to Chronic Viral Infections and Cancer. Front Immunol [Internet]. 2017 Sep 29;8:1215. Available from: https://pubmed.ncbi.nlm.nih.gov/29033936
113. Elahi S, Dinges WL, Lejarcegui N, Laing KJ, Collier AC, Koelle DM, et al. Protective HIV-specific CD8+ T cells evade Treg cell suppression. Nat Med [Internet]. 2011 Jul 17;17(8):989–95. Available from: https://pubmed.ncbi.nlm.nih.gov/21765403
114. Elahi S, Shahbaz S, Houston S. Selective Upregulation of CTLA-4 on CD8+ T Cells Restricted by HLA-B*35Px Renders them to an Exhausted Phenotype in HIV-1 infection. PLoS Pathog [Internet]. 2020 Aug 6;16(8):e1008696–e1008696. Available from: https://pubmed.ncbi.nlm.nih.gov/32760139
115. Shahbaz S, Dunsmore G, Koleva P, Xu L, Houston S, Elahi S. Galectin-9 and VISTA Expression Define Terminally Exhausted T Cells in HIV-1 Infection. J Immunol [Internet]. 2020 May 1;204(9):2474 LP – 2491. Available from: http://www.jimmunol.org/content/204/9/2474.abstract
116. Shahbaz S, Xu L, Sligl W, Osman M, Bozorgmehr N, Mashhouri S, et al. The Quality of SARS-CoV-2–Specific T Cell Functions Differs in Patients with Mild/Moderate versus Severe Disease, and T Cells Expressing Coinhibitory Receptors Are Highly Activated. J Immunol [Internet]. 2021 Aug 15;207(4):1099 LP – 1111. Available from:

http://www.jimmunol.org/content/207/4/1099.abstract
117. Yang R, Sun L, Li CF, Wang YH, Yao J, Li H, et al. Galectin-9 interacts with PD-1 and TIM-3 to regulate T cell death and is a target for cancer immunotherapy. Nat Commun. 2021;
118. Le Mercier I, Chen W, Lines JL, Day M, Li J, Sergent P, et al. VISTA Regulates the Development of Protective Antitumor Immunity. Cancer Res [Internet]. 2014 Apr 1;74(7):1933–44. Available from: https://pubmed.ncbi.nlm.nih.gov/24691994
119. Mehta N, Maddineni S, Mathews II, Andres Parra Sperberg R, Huang P-S, Cochran JR. Structure and Functional Binding Epitope of V-domain Ig Suppressor of T Cell Activation. Cell Rep [Internet]. 2019;28(10):2509-2516.e5. Available from: https://www.sciencedirect.com/science/article/pii/S2211124719309775
120. Nowak EC, Lines JL, Varn FS, Deng J, Sarde A, Mabaera R, et al. Immunoregulatory functions of VISTA. Immunol Rev [Internet]. 2017 Mar;276(1):66–79. Available from: https://pubmed.ncbi.nlm.nih.gov/28258694
121. Lines JL, Pantazi E, Mak J, Sempere LF, Wang L, O'Connell S, et al. VISTA is an immune checkpoint molecule for human T cells. Cancer Res [Internet]. 2014 Apr 1;74(7):1924–32. Available from: https://pubmed.ncbi.nlm.nih.gov/24691993
122. Mulati K, Hamanishi J, Matsumura N, Chamoto K, Mise N, Abiko K, et al. VISTA expressed in tumour cells regulates T cell function. Br J Cancer [Internet]. 2019;120(1):115–27. Available from: https://doi.org/10.1038/s41416-018-0313-5
123. Gameiro A, Nascimento C, Correia J, Ferreira F. VISTA Is a Diagnostic Biomarker and Immunotherapy Target of Aggressive Feline Mammary Carcinoma Subtypes. Cancers (Basel) [Internet]. 2021 Nov 5;13(21):5559. Available from: https://pubmed.ncbi.nlm.nih.gov/34771722
124. Kondo Y, Ohno T, Nishii N, Harada K, Yagita H, Azuma M. Differential contribution of three immune checkpoint (VISTA, CTLA-4, PD-1) pathways to antitumor responses against squamous cell carcinoma. Oral Oncol [Internet]. 2016;57:54–60. Available from: https://www.sciencedirect.com/science/article/pii/S1368837516300252
125. Wu L, Deng W-W, Huang C-F, Bu L-L, Yu G-T, Mao L, et al. Expression of VISTA correlated with immunosuppression and synergized with CD8 to predict survival in human oral squamous cell carcinoma. Cancer Immunol Immunother [Internet]. 2017;66(5):627–36. Available from: https://doi.org/10.1007/s00262-017-1968-0
126. Deng J, Li J, Sarde A, Lines JL, Lee Y-C, Qian DC, et al. Hypoxia-Induced VISTA Promotes the Suppressive Function of Myeloid-Derived Suppressor Cells in the Tumor Microenvironment. Cancer Immunol Res [Internet]. 2019 Jul 1;7(7):1079 LP – 1090. Available from: http://cancerimmunolres.aacrjournals.org/content/7/7/1079.abstract
127. Huang H, Ostroff GR, Lee CK, Agarwal S, Ram S, Rice PA, et al. Relative Contributions of Dectin-1 and Complement to Immune Responses to Particulate β-Glucans. J Immunol [Internet]. 2012 Jul 1;189(1):312 LP – 317. Available from: http://www.jimmunol.org/content/189/1/312.abstract
128. Qiu X, Chan ASH, Jonas AB, Kangas T, Ottoson NR, Graff JR, et al. Imprime PGG, a yeast β-glucan PAMP elicits a coordinated immune response in combination with anti-PD1 antibody. J Immunol [Internet]. 2016 May 1;196(1 Supplement):214.16 LP-214.16. Available from: http://www.jimmunol.org/content/196/1_Supplement/214.16.abstract
129. Zhang M, Kim JA, Huang AY-C. Optimizing Tumor Microenvironment for Cancer Immunotherapy: β-Glucan-Based Nanoparticles [Internet]. Vol. 9, Frontiers in

Immunology . 2018. p. 341. Available from: https://www.frontiersin.org/article/10.3389/fimmu.2018.00341
130. Zaretsky JM, Garcia-Diaz A, Shin DS, Escuin-Ordinas H, Hugo W, Hu-Lieskovan S, et al. Mutations Associated with Acquired Resistance to PD-1 Blockade in Melanoma. N Engl J Med [Internet]. 2016/07/13. 2016 Sep 1;375(9):819–29. Available from: https://pubmed.ncbi.nlm.nih.gov/27433843
131. Moynihan KD, Opel CF, Szeto GL, Tzeng A, Zhu EF, Engreitz JM, et al. Eradication of large established tumors in mice by combination immunotherapy that engages innate and adaptive immune responses. Nat Med [Internet]. 2016/10/24. 2016 Dec;22(12):1402–10. Available from: https://pubmed.ncbi.nlm.nih.gov/27775706